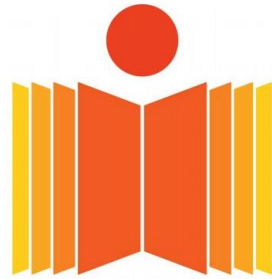# Study of fatigue damage mechanisms in composites: Numerical and experimental investigation

Milind Talele

A Thesis Submitted to

Indian Institute of Technology Hyderabad

In Partial Fulfillment of the Requirements for

The Degree of Master of Technology

भारतीय प्रौद्योगिकी संस्थान हैदराबाद
Indian Institute of Technology Hyderabad

Department of Mechanical and Aerospace Engineering

July 2015

Declaration

I declare that this written submission represents my ideas in my own words, and where ideas or words of others have been included, I have adequately cited and referenced the original sources. I also declare that I have adhered to all principles of academic honesty and integrity and have not misrepresented or fabricated or falsified any idea/data/fact/source in my submission. I understand that any violation of the above will be a cause for disciplinary action by the Institute and can also evoke penal action from the sources that have thus not been properly cited, or from whom proper permission has not been taken when needed.
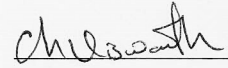
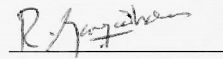_(Signature)_

Milind Talele

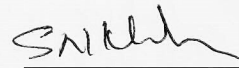(Milind Talele)

ME13M1011

(Roll No.)

Approval Sheet

This Thesis entitled Study of fatigue damage mechanisms in composites: Numerical and experimental investigation by Milind Talele is approved for the degree of Master of Technology from IIT Hyderabad

(Dr. Viswanath Chinthapenta, Asst. professor) Examiner
Dept. of Mechanical and Aerospace Engineering
IITH

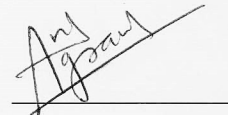(Dr. Gangadharan Raju, Asst. professor) Examiner
Dept. of Mechanical and Aerospace Engineering
IITH

(Dr. Syed Nizamuddin Khaderi, Asst. professor) Examiner
Dept. of Mechanical and Aerospace Engineering
IITH

(Dr. M. Ramji, Asso. professor) Adviser
Dept. of Mechanical and Aerospace Engineering
IITH

(Dr. Anil Agarwal, Asst. professor) Chairman
Dept. of Civil Engineering
IITH

Acknowledgements

Dedication

Dedicated to
My beloved family

Abstract

The use of fiber reinforced polymer composites for structural application is increasing nowadays. They have very high strength to weight ratio. This property justifies their use in many domains. The tensile and compressive behaviour of composite laminates is studied extensively over past decades. But fatigue in composite structures is comparatively new area and is still under development. In this work both numerical as well as experimental fatigue analysis of composite structures is carried out. The numerical model is based on strength and stiffness degradation of laminates. The fatigue progressive damage model (FPDM) is implemented in FEA to predict the life of the laminate as well as to study the progressive damage under constant amplitude fatigue load. The strength and stiffness degradation is predicted using FEA. The methodology to implement the delamination model in composites under quasi static as well as fatigue loading conditions is discussed. This model makes use of fatigue crack growth rule to model the delamination. The cohesive zone model is implemented as the interface element for delamination growth prediction. The interlaminar fracture toughness is evaluated for unidirectional Glass fiber laminates as per ASTM D5528 and ASTM D7905 standards. The experimental study is carried out on glass fiber laminates without and with hole. The interrupted testing procedure is employed to find out the residual strength as well as residual stiffness of laminates. Also the damage progression in laminates is observed through the Infrared thermography. The FPDM model implemented shows the similar trend of strength and stiffness degradation as seen from experiments. However, the delamination model needs to be improved further making it more stable towards convergence for accurate prediction.

Contents

List of Figures

List of Tables

Chapter 1

Importance of study of fatigue damage

1.1 Introduction

Invention of composite materials has revolutionized the research and development in material world. Almost all the applications where light weight and high strength is required, the composites are preferred. Composites have large applications in fields like aerospace, military, marine, wind turbines, sports equipments, civil structures etc. It is possible to create high specific strength and high specific weight components towards structural applications.

Composites can be described as materials consisting of two or more components with distinct properties and distinct boundaries between them [9]. There can be again the classifications as fiber reinforced composites and particulate composites. In any composite there should be one matrix phase and one or more reinforcement phases. The reinforcement enhances the load carrying properties of matrix or it can itself be the load carrying member.
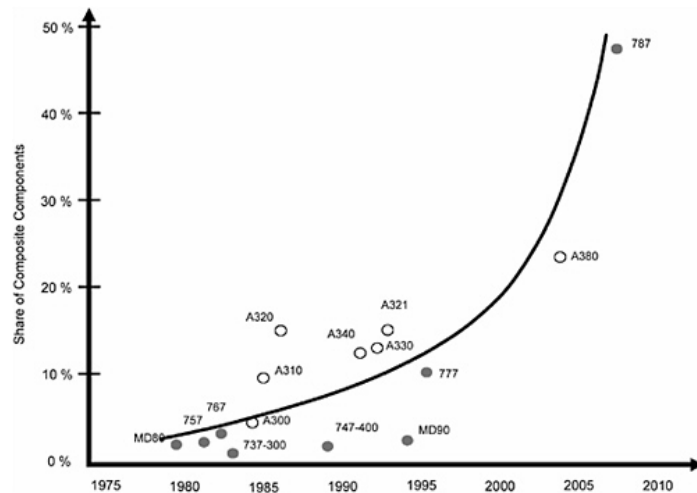
Figure 1.1: Civil aircraft composite content (% of structural weight) [1]

Mostly fiber reinforced polymer (FRP) composites are extensively used in structural applications

and this thesis mainly focuses on it. In these composites, matrix phase is generally a polymer and reinforcement phase in fibers. Carbon and glass fibers are mainly used as reinforcement but other types of fibers can also be used based on applications. FRPs have low weight, high stiffness and high strength which are essential in aerospace industry. Besides their properties can also be custom tailored. They also have possibility to integrate sensors or actuators, have high structural damping and have superior fatigue performance. Further, they are corrosion resistant. New composites are developed which can perform at elevated temperatures. Therefore we can see high use of composites in modern aerospace industry. Figure 1.1 shows the increasing trend of composite usage in civil aircraft industry. The percentage of composites in aircrafts was around 10% in the 1990's which is shooting up around 40-50% nowadays [1]. Military aircrafts have to sustain much larger and fluctuating loads as compared to civil aircrafts. Therefore similar trend can be seen in case of military aircrafts.

Besides aerospace industry many other industries are using composites as replacement for conventional metal parts. Most of the marine structures make use of composite materials because of their light weight and resistance to corrosion. They also have high acoustic transparency. This resulted in their use in SONAR domes [10]. Automobile industries are also using composites for improving the efficiency of vehicle. Most of leading automobile manufacturers are using Carbon fiber composites to manufacture chassis and many other parts of cars. Composites are integral part of formula one racing cars as weight reduction in such cars directly improves the performance. Many sports equipments like bicycles, racquets, pole vaults, golf clubs etc use composite materials to improve the performance. Owing to the increasing usage, a systematic study of composite's mechanics and their failure is of utmost importance.

1.1.1   Fatigue damage in composites

Fatigue is the process of weakening of material because of repeatedly applied load. Structures subjected to repeated cyclic load undergoes a progressive damage. This progressive damage results in reduction of stiffness and strength of the component. Thus the component or part may fail at stress levels below their design strength. Therefore, any moving part or component is prone to fatigue induced damage.

Fatigue loading is generally characterized by maximum value of applied stress, variation in the applied load, load ratio and number of cycles. The general types of fatigue loading based on these parameters are shown in the Fig. 1.2. The first loading is the fully reversed loading scenario. During this kind of loading, the component undergoes cyclic tensile and compressive loading. This type of loading is critical because of the introduction of compressive load. The compressive strength of laminates is less as compared to tensile case. The second one is Tensile-Tensile loading in which both upper and lower stress levels are in the tensile region. Similarly both load levels could be compressive as well. This loading is characterized by the positive stress ratio.

Fatigue in metals is studied extensively and mostly understood. The fatigue data for most of the metals is well documented too. The fatigue damage in metals starts from a single dominant crack and its propagation till the final failure. While in case of high cycle fatigue, the material hardening is observed. But the fatigue damage mechanism in composites is totally different as damage mechanism is completely different from metals and they are quite complex. Lot of factors can affect the fatigue
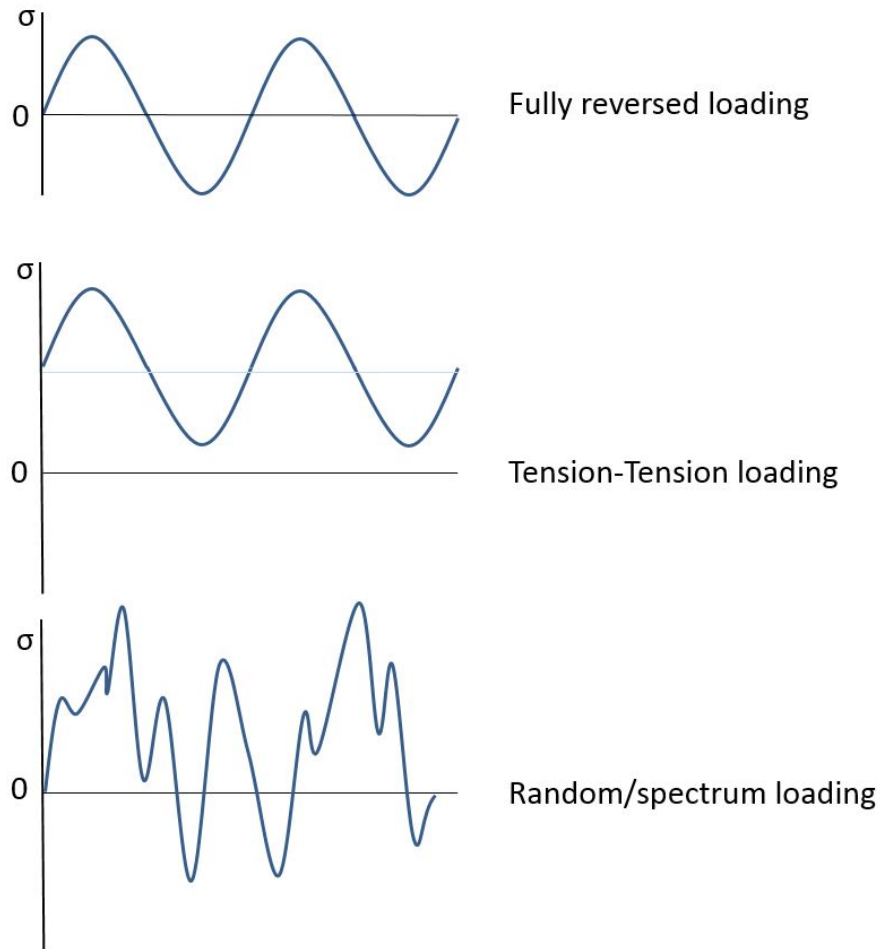
Figure 1.2: Fatigue loading cycles

response of composites. It can get affected by type of fibers, matrix, manufacturing method, curing cycle, stacking sequence etc. Unlike metals, the fatigue damage in composites starts with multiple matrix cracks. However, some microstructural failure mechanisms also take place during the damage in composites. Fiber breakage, matrix cracking, fiber-matrix shear out and delamination take place during damage evolution. All of these mechanisms occur either independently or sometimes they interact with each other. This makes the fatigue analysis and progressive damage prediction of composite structure a difficult and complex job.

1.1.2 Delamination in composites

Delamination is basically the failure of interlaminar interface between the adjacent laminae. It is one of the important mode of damage which develops and grows under fatigue loading. This failure generally results in the separation of the laminae. There are various causes for the delamination to be introduced in the composite components. Some of them are impact, fatigue loading etc. While the composites have very good strength in the fibers direction, they have very low resistance to the delamination as their strength is very poor along the thickness direction. Generally three modes of

3

Figure 1.3: Multiple delaminations in CFRP

delamination are observed in composites. i) mode 1: where the force acting normal to the interface causes the separation, ii) mode 2: where shear force acting on interface causes the separation and iii) mode 3: where tearing under shear is observed. The schematics of these loading modes is shown in Fig. 1.4. However, these modes very rarely occur individually. In most of the cases, the mode mixity is observed. Due to the complex interactions between the modes, the delamination modelling is a challenging task. It becomes more difficult in case of quasi-isotropic laminates where each layer has different fiber orientation. Even if the initial delamination is not present in the laminate, it may originate and propagate under service loads. It is assisted by the fatigue loading. Matrix cracks, disbonds and other failures also act as the initiator for the delamination. Nowadays lot of research is focussed on accurate modeling of delamination growth under fatigue loading. The delamination study can be categorized in two parts.

i) quasi static delamination

ii) fatigue delamination.

(a) mode-I   (b) mode-II   (c) mode-III
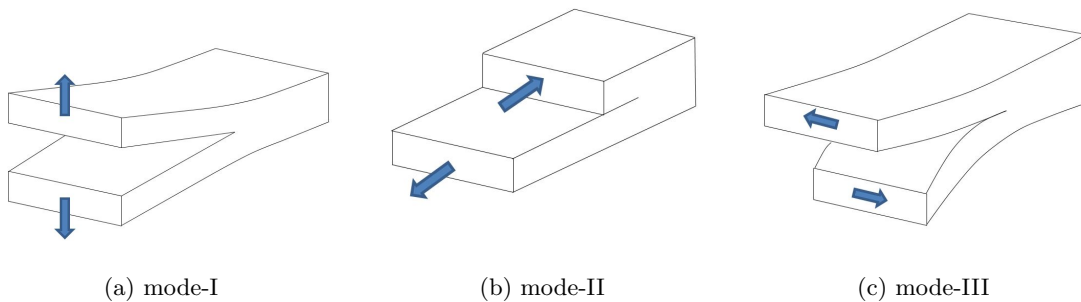
Figure 1.4: Modes of delamination [2]

The delaminations propagating under monotonic increasing loading are termed as quasi static delamination. The delaminations for which the main driving force is fatigue loading are termed as

fatigue delamination. The analysis of fatigue delaminations is more difficult as the accurate data related to the fatigue crack growth is required and further initial delamination parameters degrade with cycles.

1.2 Literature reviews

1.2.1 Progressive damage modelling in composites

The fatigue damage modelling is the complicated task as previously discussed. This is because of the damage growth due to static as well as fatigue mechanisms. Many researchers have developed the finite element models to predict the damage growth in composite laminates. Hashin [11] presented the failure criteria is one of the initial works related to the fatigue failure mechanisms. Other criterions like Tsai-Wu, Tsai-Hill, Hoffman, Puck failure criteria are developed and successfully implemented. Chang et al [12] have developed the progressive damage model for composites with stress concentrations. They have made use of material property degradation rules for simulating the damage in composites under quasi static loading. There are three steps involved in this process. They are stress analysis, damage prediction by failure criterions, and damage modelling. Many researchers have used the same methodology to predict the damage in composites. The PDM is used to predict the damage growth in composite laminates with single and multiple holes [13, 14] , the analysis of bolted joints [15], patch repair study [16] etc. Thus the PDM is well established method for quasi static loading in composite but for fatigue loading not much work has been done

1.2.2 Fatigue progressive damage modelling

The Fatigue Progressive Damage Modelling (FPDM) follows almost same path as the PDM. The failure criterions used in this case are fatigue failure criterions. The initial work in fatigue failure criterions was done by Hashin [17]. In that paper, the strength of laminates was replaced by residual strength. This failure criteria is widely used for the numerical implementation of FPDM. Shokrieh et.al. [4] developed the fatigue progressive damage model and implemented for bolted joints. This model introduced the generalized material property degradation. The data required for this model was experimentally obtained [18]. Papanikos et.al. [7] and Tserpes et.al. [19] implemented similar procedure but with addition of Ye's delamination criteria [20] along with Hashin's fatigue failure criteria. This was implemented for plate without hole and axial loading. Paepegem et.al. [21] carried out FEA based study for the bending fatigue case and compared those results with experimental data.

1.2.3 Delamimation growth study

Delamination is one of the major failure mode in composites as it cannot be easily detected but can affect their properties significantly. Thus the model which will accurately predict the delamination onset and growth needs to be developed. Initially in the literature the analysis of delamination growth was performed using fracture mechanics approach and J-Integral [22]. However, this model required initial delamination or crack to be present. Therefore the concept of cohesive zone modeling (CZM) was introduced. It was first developed by Dugdale [23]. It was later modified by Barenblatt

5

[24] and Hillerborg [25]. The cohesive zone model are able to predict the onset as well as propagation of delamination. Various forms of cohesive law are developed over the period of time. Tvergaard [26] proposed the trapezoidal law. Needleman derived the polynomial law [27] for traction seperation and later modified it to the exponential law [28]. The most commonly used models are exponential and bilinear cohesive zone models. The bilinear cohesive zone law was proposed by Mi et.al. [29].These laws are implemented and modified by many researchers [6, 8, 30, 31]. The fatigue implementation is carried out by Munoz et.al. [32]. To simulate the delamination propagation, Peerling's law [33] along with interface elements was used. Turon et.al. [34] used the concept of Paris law for delamination propagation.Similar works are carried out by Robinson et.al. [35], Naghipour et.al. [36].

1.3 Motivation, scope and objectives

Fatigue was identified as the severe cause for damage under actual service load. Both tensile and compressive behaviour of composite laminates are very well understood but its behaviour under fatigue load is not very well understood. The initial attempts in case of fatigue experiments were to find out the fatigue life of composites. The composites can undergo various load states in fatigue like tensile-tensile fatigue, tensile compressive fatigue or random loading. Thus the composites need to be tested for each loading case individually. Out of these cases, the tensile-compressive loading is the critical one as compressive strength of composites is less than its tensile strength and further damage mechanism is completely different unlike metal. Therefore, systematic study of behaviour of composite structures under fatigue loading is necessary.

One way of understanding the fatigue in composites is to undertake the experimental programs. Then based on experimental results, the analytical/mathematical models could be developed to model the fatigue life and reproduce the experimental results. Another approach is to develop numerical models to simulate the damage growth in composites and predict the fatigue life based on that. Lot of researchers have developed various numerical models for fatigue analysis of composite laminates. The numerical models can predict the residual stiffness and strength corresponding to the number of loading cycles. Similarly delamination in composites is also one of the major concern as it reduces the load carrying capacity of component. Delamination growth in composites can be characterized experimentally for individual loading modes. These growth rules can be applied in numerical simulations to predict the delamination growth in actual component under complex loading conditions. Cohesive zone modelling is one promising way to simulate the delamination growth in composites under mixed mode loading conditions. Lot of cohesive zone models are available and implemented for quasi static loading conditions. But modelling of the delamination growth due to fatigue loading is still under development.

The objective of thesis is outlined as follows:

- To study and implement the progressive damage model for composite laminates under fatigue loading by employing FEA.

- To model the cohesive zone to simulate the delamination growth in composite laminates. This is to be developed and implemented for both quasi static case as well as fatigue loading case.

- For any numerical analysis the experimental data is required towards quantitative/qualitative comparison. Therefore, one objective is to characterize the interlaminar fracture toughness for

composite laminates under quasi static loading conditions.

- The damage developed in composite laminates are very hard to detect. Therefore, infrared thermography is employed to assess the delamination growth in-situ for validating through PDM model.

1.4   Thesis layout

Chapter 1 discusses about introduction to composites, the damage mechanisms in composites and the importance of study of fatigue damage mechanisms. The brief literature survey is also provided about the topic.

Chapter 2 focusses on Finite Element Modeling aspects of fatigue in composites. The Fatigue Progressive Damage Model based on the strength and stiffness degradation is discussed. This model is implemented in FEA using software package ANSYS15. The results along with the shortcomings of this model is also discussed

Chapter 3 discusses about the cohesive zone modeling for delamination growth. The delamination growth in composites can be tracked effectively by implementation of cohesive zone modelling. The delamination model for quasi static loading as well as for a fatigue loading is presented. Same is implemented in FEA using interface element. The interlaminar fracture toughness of GFRP is evaluated experimentally following the ASTM standards.

Chapter 4 deals with the experimental aspects related to constant amplitude fatigue loading. The VARIM method used for manufacturing of composite laminates is discussed. The tests performed on GFRP specimens both without and with hole are summarised in this chapter. The infrared thermography is employed for damage assessment with increasing cycles.

Chapter 5 is the conclusion and recommendation for future work.

Chapter 2

Progressive damage modelling of composite laminates under fatigue loading

2.1 Introduction

The experimental fatigue characterization of composites is almost as old as composites themselves. However, the experimental characterization is very lengthy process. In case of large components, it is not feasible to carry out the experiments. Besides time, it would also require some specialized loading equipments. Composites being costly than most of the metals, it is impractical to go for experiments every time. So it is always better to opt for numerical simulations. Numerical simulations can predict the onset, propagation and critical value of damage in composites. Fatigue damage propagation and life can be modelled by various methods. However, most popular of them are residual stiffness and residual strength. Residual stiffness approach is more favoured because the stiffness of specimen can be measured non-destructively. In this methodology, the residual stiffness of component is used to determine the fatigue damage and life of component. However, the residual strength approach relies on the strength of specimen and thus would require large number of specimen.

2.2 Fatigue Progressive Damage Model (FPDM)

The progressive damage model (PDM) in case of composites is well developed. The FPDM also follows the same procedure as PDM. FPDM is a three stage process.1) Stress analysis, 2) Fatigue failure analysis, 3) Material property degradation

Stress analysis is carried out by linear analysis. Then the fatigue failure analysis is carried out. The Hashin's criteria [17] is used to detect the failure modes. The failure modes considered in this analysis are matrix tensile and compressive failure, fiber tensile and compressive failure and fiber matrix shear out. Along with this, Ye's criteria [20] is used to find out the delamination failure under both tensile and compressive cases. The set of rules proposed by Hashin for fatigue failure

are as follows:

- Tensile Fiber Failure, for $(\sigma_{xx} > 0)$:

$$\left(\frac{\sigma_{xx}}{X_T^F}\right)^2 + \frac{\sigma_{xy}^2 + \sigma_{xz}^2}{\left(S_{12}^F\right)^2} \geq 1 \tag{2.1}$$

- Compressive Fiber Failure, for $(\sigma_{xx} < 0)$:

$$\left(\frac{\sigma_{xx}}{X_C^F}\right)^2 \geq 1 \tag{2.2}$$

- Tensile Matrix Failure, for $(\sigma_{yy} > 0)$:

$$\frac{(\sigma_{yy} + \sigma_{zz})^2}{\left(Y_T^F\right)^2} + \frac{\sigma_{yz}^2 - \sigma_{yy}\sigma_{zz}}{\left(S_{23}^F\right)^2} + \frac{\sigma_{xy}^2 + \sigma_{xz}^2}{\left(S_{12}^F\right)^2} \geq 1 \tag{2.3}$$

- Compressive Matrix Failure, for $(\sigma_{yy} < 0)$:

$$\left[\left(\frac{Y_C^F}{2S_{23}^F}\right)^2 - 1\right]\left(\frac{\sigma_{yy} + \sigma_{zz}}{Y_C^F}\right) + \frac{(\sigma_{yy} + \sigma_{zz})^2}{4\left(S_{23}^F\right)^2} + \frac{\sigma_{yz}^2 - \sigma_{yy}\sigma_{zz}}{\left(S_{23}^F\right)^2} + \frac{\sigma_{xy}^2 + \sigma_{xz}^2}{\left(S_{12}^F\right)^2} \geq 1 \tag{2.4}$$

- Fiber matrix shear out, for $(\sigma_{xx} < 0)$:

$$\left(\frac{\sigma_{xx}}{X_C^F}\right)^2 + \left(\frac{\sigma_{xy}}{S_{xy}^F}\right)^2 + \left(\frac{\sigma_{xz}}{S_{xz}^F}\right)^2 \geq 1 \tag{2.5}$$

And the rules proposed by Ye for delamination are as follows:

- Delamination in tension, for $(\sigma_{zz} > 0)$:

$$\left(\frac{\sigma_{zz}}{Z_T^F}\right)^2 + \left(\frac{\sigma_{xz}}{S_{31}^F}\right)^2 + \left(\frac{\sigma_{yz}}{S_{23}^F}\right)^2 \geq 1 \tag{2.6}$$

- Delamination in compression, for $(\sigma_{zz} < 0)$:

$$\left(\frac{\sigma_{zz}}{Z_C^F}\right)^2 + \left(\frac{\sigma_{xz}}{S_{31}^F}\right)^2 + \left(\frac{\sigma_{yz}}{S_{23}^F}\right)^2 \geq 1 \tag{2.7}$$

The superscript 'F' in the above terms represents the fatigue properties. This suggests the residual strength of the component. It is observed that as the fatigue cycles increase, the stiffness as well as the strength of component goes on decreasing. Therefore next part of FPDM is material property degradation. In this, the properties of failed element are degraded preventing it to carry the further load. The degradation in case of fatigue is discussed in the next section.

9

2.3 Generalized property degradation rules

In previous section, various failure criteria are discussed. Some of these are catastrophic while some of them are not. This can be modelled by degrading the corresponding properties of element. There are two types of degradation observed in case of fatigue loading. Sudden degradation and gradual degradation. The sudden degradation can be explained by the case of monotonic loading. When the load is increased monotonically, at some particular load level, the element may fail by one or more failure criteria as mentioned in failure criteria. This is modelled by sudden material property degradation. However, if no failure is detected, the material keeps on degrading slowly because of the effect of fatigue loading. Both of these damage models are discussed here.

2.3.1 Sudden property degradation

Once the failure is detected in any element, the properties of the failed region of the laminate must be changed. Therefore the failed element can be replace by the identical element with degraded material properties. Thus the conventional stress analysis can again be applied. However, the degradation of failed is not a random process. Each failure has different effect on the properties of composites. There are various degradation rules available in literature [37, 38]. The degradation rules proposed by McCarthy et.al. [39] are used in this study. These degradation rules are summarised in the table below.

Failure mode	E_{xx}	E_{yy}	E_{zz}	G_{xy}	G_{yz}	G_{xz}	ν_{xx}	ν_{yz}	ν_{xz}
Tensile fiber failure	X			X		X	X		X
Compressive fiber failure	X			X	X	X	X		X
Tensile matrix failure		X	X		X			X	
Compressive matrix failure		X	X		X			X	
Delamination in tension			X		X	X		X	X
Delamination in compression			X		X	X		X	X
More than 1 failure	X	X	X	X	X	X	X	X	X

Table 2.1: Degradation rules for various modes of failure

When the tensile or compressive fiber failure takes place, the element fails to take load in the fiber direction as fiber is the main load carrying member in this direction. Thus all the properties in this direction are degraded. Fiber failure is catastrophic. Matrix cracks are generated along the fiber direction. Thus the material loses load carrying capacity in yy and zz direction. But all the properties in xx direction are retained. When the delamination failure is detected, the material cannot take load in zz direction as well as it loses capacity to transfer shear load. Therefore corresponding properties are degraded. Once more than 1 failures are detected at some region, all the properties are degraded for that material.

2.3.2 Gradual stiffness degradation

The residual stiffness of composite laminate subjected to fatigue loading can be used to characterize the life of component. Lot of studies have been performed for the stiffness degradation under fatigue loading. These studies suggested that the stiffness degradation in fiber composites is insignificant. The composites retain large percentage of their initial stiffness till the end of their fatigue life. Linear degradation of stiffness is observed in case of composites. This degradation is the result of accumulation of matrix cracks. As the number of cycles go on increasing, these cracks grow in size as well as in number. Thus the load bearing capacity of composites goes on decreasing slowly.
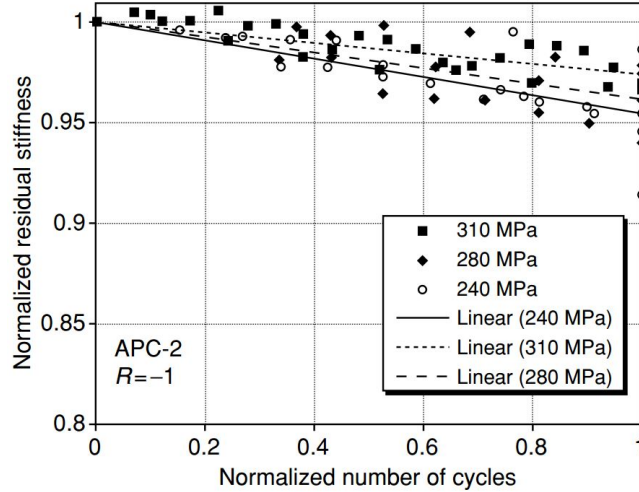
Figure 2.1: Normalised residual stiffness of APC-2 laminate [3]

Figure 2.1 shows the stiffness degradation curve for APC-2 carbon fiber laminate taken from Ref. [3]. One can see that stiffness at the end of life is above 95% of initial stiffness. Also this degradation is not affected much by the magnitude of fatigue load being applied. This can be incorporated in the FEA code by fitting linear curve to this data. This equation can be expressed as:

$$E\left(n\right) = \left[A\left(\frac{n}{N_f}\right) + 1\right] E_s \tag{2.8}$$

where n is the current number of cycles, N_f is the number of cycles till failure, $E\left(n\right)$ and E_s are the residual and initial stiffness of laminate. A is the experimental curve fitting parameter.

2.3.3 Gradual strength degradation

As the damage starts accumulating in the laminate due to fatigue, the ultimate tensile strength is also affected. This effect is also captured by the interrupted fatigue tests. However, destructive tests need to be carried out on specimen to get the gradual strength degradation. The effect of fatigue on strength is much severe than that on stiffness as depicted from fig 2.2. However, in this case also it can be seen that the normalised strength degradation has very low effect of maximum value of stress in cycle. The fitted curve for the data almost follow the same path. The second degree
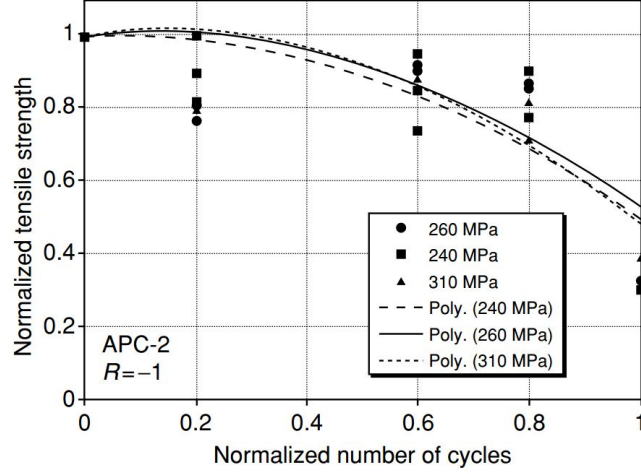
Figure 2.2: Normalised residual strength of APC-2 laminate [3]

equation is fitted to the data as follows:

$$T\left(n\right) = \left[B\left(\frac{n}{N_f}\right)^2 + C\left(\frac{n}{N_f}\right) + 1\right]T_s \tag{2.9}$$

where $T\left(n\right)$ and T_s are residual and initial static strength of laminate, n is the current number of cycle, N_f is the final number of cycles till the failure. This equation is normalised in terms of number of cycles and thus can be applied to any maximum load as long as load ratio remains same.

2.4 Finite Element Modeling of FPDM

The previously discussed formulation for fatigue progressive damage modeling is implemented in FEA. The standard software package ANSYS 15 is used for his purpose. The 16-noded SOLID186 element is chosen for modeling. The length and width of laminate is 150 mm and 26 mm respectively. Eight layers are modelled each having thickness of 0.25mm making the total thickness of laminate as 2 mm. The stacking sequence chosen is $[45/0/-45/90]_s$. The mesh size of laminate is 75 through length $\times$ 13 through width $\times$ 8 layers.
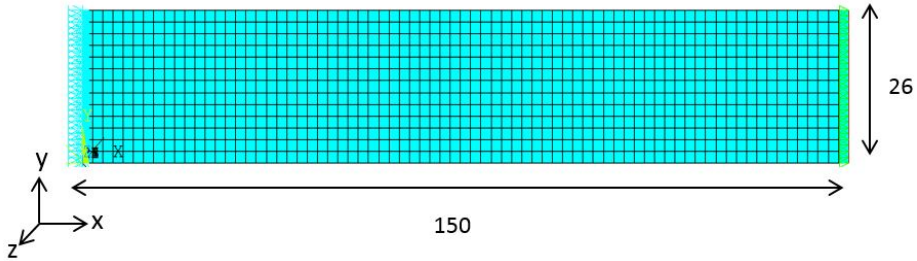
Figure 2.3: Finite element model for composite laminate

The flowchart shown in the fig 2.4 is followed for analysis. The linear analysis is carried out
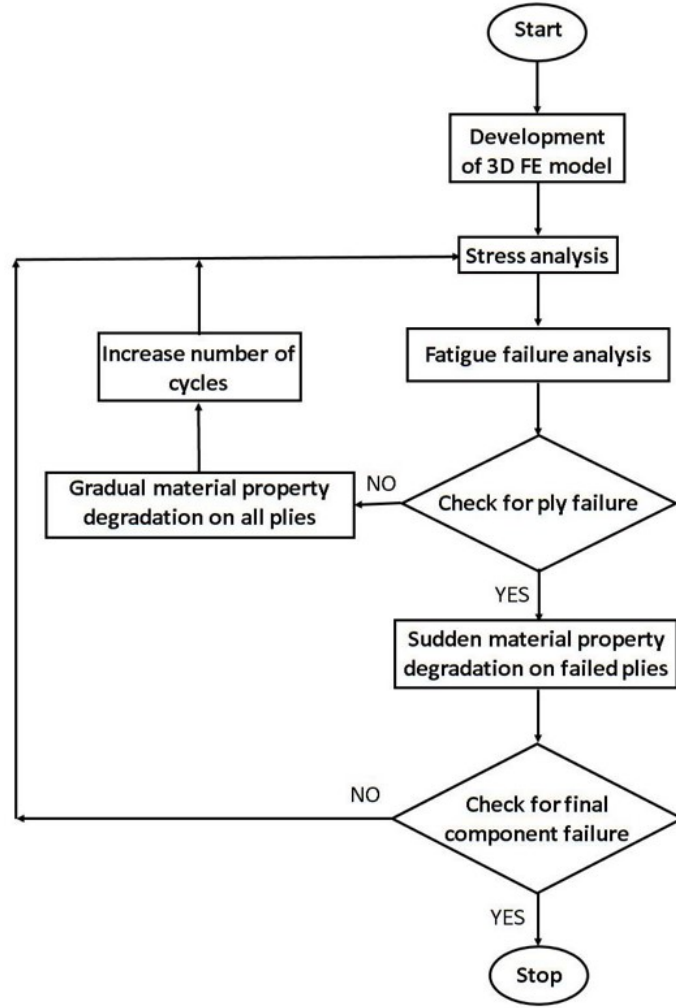
Figure 2.4: Flowchart for fatigue progressive damage modeling [4]

in the ANSYS package. The stress values are stored. Then the elements are checked for failure against failure criteria mentioned in eq 2.1-2.7. Once the failure is detected by any failure criteria, the corresponding properties are degraded by sudden degradation rule as given in table 2.1. Once the degradation is complete, the analysis is run at same number of cycles to check the progressive damage till no failure is detected. Then the number of cycles is increased by Δn. In this case, the gradual degradation rules are applied as per eq 2.8 and eq 2.9. The values of experimental constants are found out to be $A = -0.05$, $B = -0.5536$ and $C = 0.105$. The negative values of A and B suggest that the material is undergoing degradation. Table 2.2 shows the properties of composite material. All the degrees of freedom of laminate are arrested on left side while the load applied on the right side nodes. The modelling of cyclic load is also one the most critical aspect of FPDM. The most accurate results may be obtained by modelling the complete cycle. However, the analysis is to be run for several times. Thus it would be computationally inefficient to model the complete cycle. Thus only maximum and minimum loads in the cycle are applied. So it is assumed that the damage in the laminate occur at these extremities. Further modelling each cycle is also inefficient and the analysis consumes lot of time. Therefore cycle jump strategy is employed. So instead of

13

Material property	values
E_{xx}	134 GPa
$E_{yy} = E_{zz}$	8.9 GPa
$G_{xy} = G_{xz}$	5.1 GPa
G_{yz}	3.0 GPa
$\nu_{xy}, \nu_{xz}, \nu_{yz}$	0.28
X_T	2130 MPa
$Y_T = Z_T$	80 MPa
$Y_C = Z_C$	1100 MPa
$S_{xy} = S_{xz}$	16 MPa
S_{yz}	14 MPa

Table 2.2: Properties of APC-2 carbon fiber laminate [7]

modelling each and every cycle, the number of cycles are incremented by suitable Δn. This reduces the computational load. The modelling, analysis and post processing are implemented in ANSYS using the APDL code. The results of this model are discussed in the next section.

2.5   Results and discussion

Figure 2.5 shows the progressive damage taking place in the laminate. The load applied is 240 MPa with load ratio of -1. The fatigue life of laminate is found out to be 12,40,000 cycles. The damage can be seen to propagate rapidly in the final stages. This can be justified by the fact that as number of cycles increase, the stiffness and strength of laminate goes on reducing.
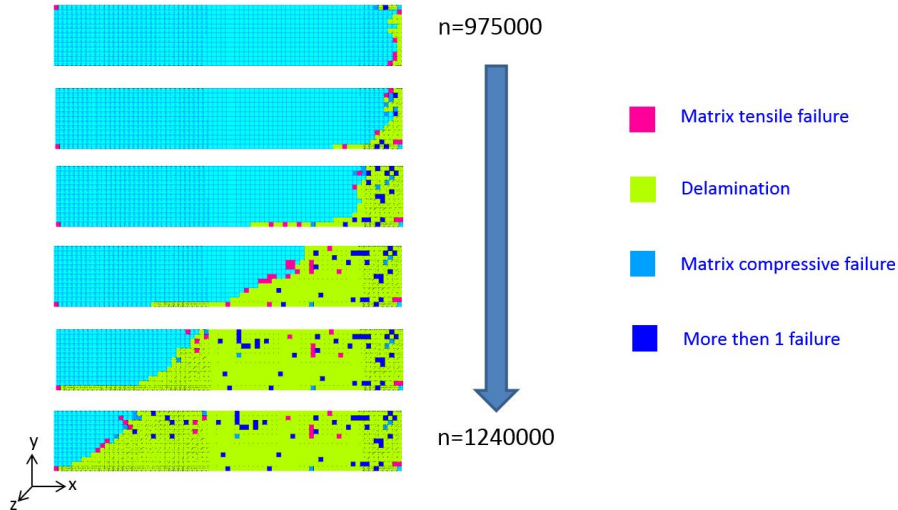
Figure 2.5: The damage progression observed through FPDM
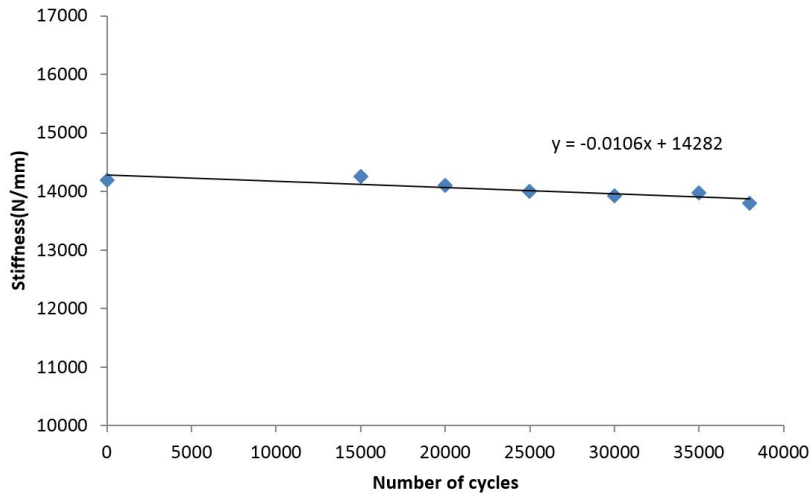
Figure 2.6: Stiffness degradation of laminate

Thus the failure criteria can detect the sudden failures in this stage of life. As it can be seen from the fig 2.5, the main mode of failure detected is the delamination along with some fiber failure at the end stage. However, as mentioned in references, the delamination should always initiate from the stress free edges of laminate. This phenomenon is not correctly captured using this model. Similarly Ye's delamination criteria failed to predict the interlaminar delamination as the elements on both sides of the interface don't fail simultaneously. The failure criteria is applied for each layer and thus it can detect the intra-laminar delamination.
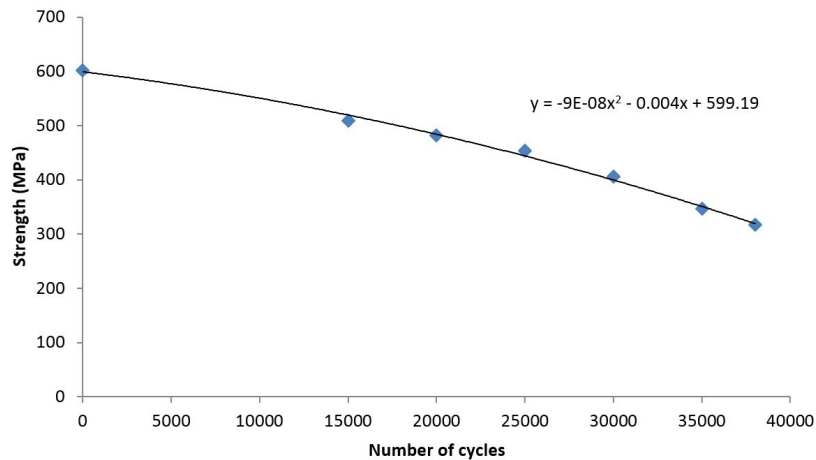
Figure 2.7: Strength degradation of laminate

However, the model was able to capture the stiffness and strength degradation trends. Thus the same simulations are carried out but with interrupted static tests. In these simulations, cyclic load is applied for number of cycles as mentioned in table 2.3 and then quasi static analysis is performed in order to find out the residual stiffness and residual strength of the laminate. The same stacking sequence is chosen for these simulations. The dimensions of laminate are $150 \times 25 \times 2$ mm. The maximum stress applied in each cycle is 300 MPa. The stress ratio chosen is 0.1. It is a tensile tensile fatigue cycle with maximum stress of 300 MPa and minimum stress of 30 MPa.

15

The quasi static test is performed on undamaged laminate to get the initial stiffness and strength. Then the fatigue cycles are applied to the laminate. The results of the simulations are summarised in the Table 2.3. It can be seen that the trends for stiffness and strength are same as those reported in literature. Figure 2.6 shows the stiffness degradation trend. The stiffness degrades linearly with the number of cycles and laminate almost retains 90% of the stiffness at the end of fatigue. Figure 2.7 shows the degradation of strength of laminate as number of cycles increase. The strength degradation shows the nonlinear degradation as reported in literatures.

Number of cycles	Stiffness (N/mm)	Strength MPa
0	14194	602
15000	14258	509
20000	14107	482
25000	13999	453
30000	13929	406
35000	13971	346
38000	13797	317

Table 2.3: Strength and stiffness degradation of laminate as observed through FPDM

2.6 Closure

The progressive damage model for fatigue loading is implemented in FEA. The implemented model can predict various modes of failure as well as it can be employed to assess the progressive damage in the composite laminate under constant amplitude fatigue loading. However, Ye's delamination criteria is unable to predict the delamination growth accurately. The interlaminar delamination has not been achieved as the model implemented is based on elementwise failure criteria. The delamination predicted consists of only intralaminar damage only. Therefore, the model needs to be refined or the cohesive zone modelling should be implemented to track the delamination growth. However, the implemented model is able to predict the stiffness and strength degradation correctly. The trends for fatigue degradation of properties is very similar to the trends reported in the literatures. In the next chapter delamination growth under fatigue loading is modelled using CZM approach.

Chapter 3

Delamination growth modeling in composite laminate under cyclic loading using FEA

3.1 Introduction

Delamination in composite laminates is one of the most significant mode of failure as it is very hard to detect the subsurface delaminations. The structural bending stiffness is adversely affected by delamination. Also if delamination can produce local buckling in structure under compressive loads. As explained in section 1, there are three basic modes of delamination. Mode I, mode II and mode III. Each of these modes can be represented by the traction separation law. Figure 3.1 shows the
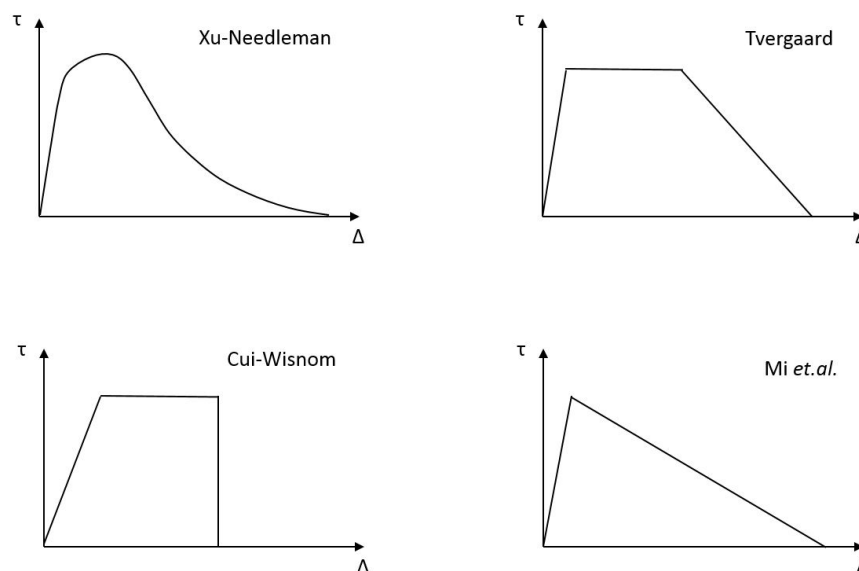
Figure 3.1: Various models for cohesive zone laws [5]

17

cohesive laws proposed in literatures [26,28,29]. Though lot of cohesive zone models are proposed by many authors , the bilinear law is most preferred as it resembles closely to the actual phenomenon of delamination. Figure 3.2 shows the traction separation graph for the bilinear cohesive zone law. As shown in the figure, the bilinear cohesive zone model is characterized by high initial stiffness
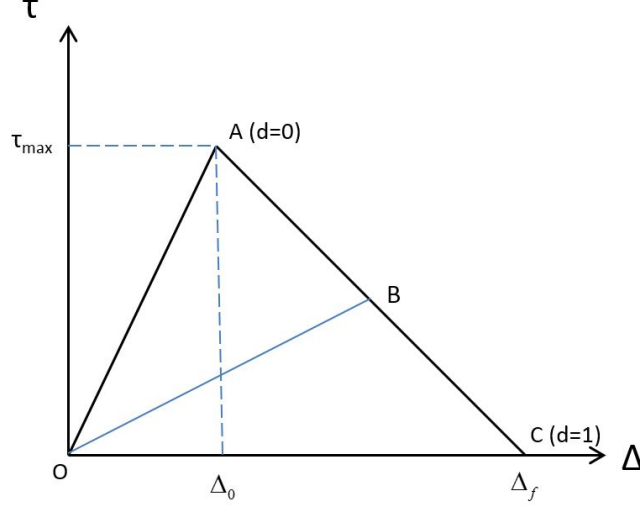
Figure 3.2: Bilinear Cohesive Zone Law

and then linear softening. The high initial stiffness ensures the perfect contact between the surfaces. When the traction reaches τ_{max}, the interface damage starts to take place and it starts opening. The area under the traction separation curve is equal to the fracture toughness G_c. When the energy absorbed by interface becomes equal to the fracture toughness, the interface fails completely and it cannot take any load. Thus the damage index 'd' ie zero at the start of delamination (point A) and is equal to 1 at the end of delamination (point C). However, if the loading is stopped at point B and then unloaded, at the next loading cycle, the traction separation curve follows path O-B-C. This is result of the damage in the previous step which is irreversible.

3.2 Mixed mode delamination

Various modes of delamination co-exist for almost all types of loading. The G_c values for different modes are also different. Therefore it is needed to develop the equivalent CZM which will take into account all the existing modes of delamination. The basic mixed mode onset criteria can be derived from Ye's criterion [20] as follows:

$$\left(\frac{\langle\tau_1\rangle}{\tau_1^0}\right)^2 + \left(\frac{\tau_2}{\tau_2^0}\right)^2 + \left(\frac{\tau_3}{\tau_3^0}\right)^2 = 1 \tag{3.1}$$

where τ_1 denotes normal traction and τ_2 & τ_3 denote the shear tractions. $\langle.\rangle$ is the MacAuley bracket defined as $\langle x\rangle = \frac{1}{2}\left(x + |x|\right)$. As the MacAuley bracket gives zero value for negative input, it is ensured that the normal separation will occur under positive normal traction only. The negative normal traction will not have any effect on the delamination model. The propagation criteria can

18

be defined by the power law expression as

$$\left(\frac{G_I}{G_{Ic}}\right)^{\alpha} + \left(\frac{G_{II}}{G_{IIc}}\right)^{\beta} + \left(\frac{G_{III}}{G_{IIIc}}\right)^{\gamma} = 1 \tag{3.2}$$

in this criteria, G_I, G_{II}, G_{III} represent the corresponding components of energy release rate. α, β, γ are the experimental constants. If $\alpha = \beta = \gamma = 1$, it is linear failure criteria and $\alpha = \beta = \gamma = 2$ gives quadratic failure criteria. Quadratic failure criteria is generally chosen when no experimental values of constants are known.
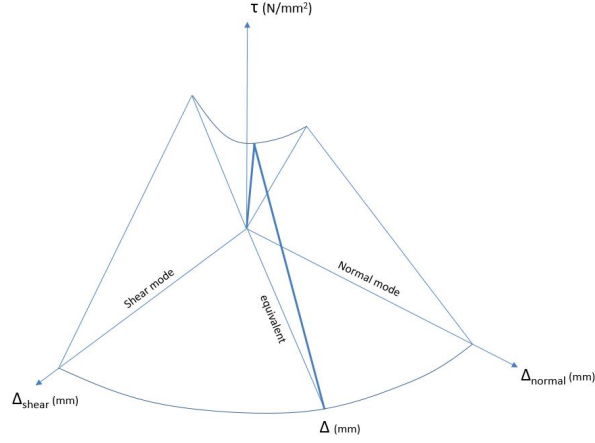
Figure 3.3: Mixed mode delamination [6]

Benzeggagh and Kenane [40] carried out lot of experimental work for the delamination growth under mixed mode loading. Based on the experimental data they proposed the general expression for critical energy release rate as

$$G_c = G_{Ic} + (G_{IIc} - G_{Ic})\left(\frac{G_{shear}}{G_T}\right)^{\eta} \tag{3.3}$$

Thus the delamination grows when total energy release rate G exceeds the critical value G_c. The energy release rate G under mixed mode is defined as $G = G_I + G_{shear}$ and $G_{shear} = G_{II} + G_{III}$. The area under the traction separation curve is equal to the corresponding fracture toughness. Therefore

$$G_c = \frac{1}{2}K\Delta^0\Delta^f \tag{3.4}$$

using eq 3.4 and eq 3.3, the propagation criteria can be derived in terms of displacement jump as

$$\Delta^f = \frac{\Delta_1^0\Delta_1^f + \left(\Delta_{shear}^0\Delta_{shear}^f - \Delta_1^0\Delta_1^f\right)\left(\frac{G_{shear}}{G_T}\right)^{\eta}}{\Delta^0} \tag{3.5}$$

where Δ_3^0 and Δ_{shear}^f are pure mode onset displacement jumps. The ratio $\frac{G_{shear}}{G_T}$ is defined in terms

of ratio of displacement jumps as

$$B = \frac{G_{shear}}{G_T} = \frac{\beta^2}{1 + 2\beta^2 - 2\beta} \tag{3.6}$$

where,

$$\beta = \frac{\Delta_{shear}}{\Delta shear + \langle \Delta_3 \rangle} \tag{3.7}$$

Until point the final separation has been derived. But for complete modeling of bilinear CZM, the onset separation is also required. Turon *et.al.* [8] proposed the criteria for onset separation as

$$\left(\Delta^0\right)^2 = \left(\Delta_1^0\right)^2 + \left(\left(\Delta_{shear}^0\right)^2 - \left(\Delta_1^0\right)^2\right) B^\eta \tag{3.8}$$

This formulation presented above takes into account the mixed mode ratios. And thus is applicable in general loading conditions. However, this model is derived for quasi static loading condition only. The additional formulation required for implementation towards fatigue load is derived in next section.

3.3 Cohesive zone model for cyclic loading

Fatigue is the common cause of failure in composite structures. The delamination modeling in composites under fatigue loading can be done by making use of Paris law. In this law, the fatigue crack growth rate is described as

$$\frac{\partial A}{\partial N} = C \left(\frac{\Delta G}{G_c}\right)^m \tag{3.9}$$

where A is the crack area or in case of delamination, it represents the delamination area. N is the umber of cycles. C and m are experimental constants which depend on the mode mixity ratio. This eq 3.9 can be introduced in the formulation of cohesive zone model to grow the delamination front as number of cycles increase. Authors Naghipour *et.al.* [36] and Turon *et.al.* [34] ahve implemented Paris law in exponential and bilinear model of CZM. From the quasi static model, the damage variable can be obtained as

$$d = \frac{\Delta^f (\lambda - \Delta 0)}{\lambda (\Delta^f - \Delta^0)} \tag{3.10}$$

Using this damage variable, the ratio of damaged area to the total area can be obtained as

$$\frac{A_d}{A^e} = \frac{d\Delta^0}{\Delta^f (1 - d) + d\Delta^0} \tag{3.11}$$

The damage evolution criteria takes into account the damage created because of static as well as fatigue loading. Thus the total damage variable is represented as

$$\frac{dd}{dt} = \dot{d} = \dot{d}_{static} + \dot{d}_{cyclic} \tag{3.12}$$

This damage growth is presented in terms of time which is analogous with the number of cycles being applied. In this section, the formulation for cyclic loading only is presented. The cyclic

damage growth is again decomposed as

$$\frac{\partial d}{\partial N} = \frac{\partial d}{\partial A_d} \frac{\partial A_d}{\partial N} \tag{3.13}$$

where A_d is the damaged area and $\frac{\partial A_d}{\partial N}$ is the growth rate of damaged area. It is the material property. The first term $\frac{\partial d}{\partial A_d}$ canbe derived by differentiating the eq 3.11. Thus we get

$$\frac{\partial d}{\partial A_d} = \frac{1}{A^e} \frac{\left[\Delta^f (1-d) + d\Delta^0\right]^2}{\Delta^0 \Delta^f} \tag{3.14}$$

In the degradation process, the delaminated area grows by ΔA_d for ΔN cycles. This increase in damaged area is the effect if increase in damage in all elements ahead of delamination front. The sum of areas of elements ahead of delamination front is equal the area of cohesive zone. Therefore the total crack growth rate can be given as sum of all individual crack growth rates in elements.

$$\frac{\partial A}{\partial N} = \sum_{e \in A_{cz}} \frac{\partial A_d^e}{\partial N} \tag{3.15}$$

here A_d^e represent the damaged area of one element in cohesive zone and A_{cz} is the total area of cohesive zone. Assuming the area of one element in cohesive zone is equal to A^e, the above equation can be rewritten as

$$\frac{\partial A}{\partial N} = \frac{A_{cz}}{A^e} \frac{\partial A_d}{\partial N} \tag{3.16}$$

Therefore the ratio $\frac{A_{cz}}{A^e}$ represents the number of elements in the cohesive zone. Using eq. 3.16, the damage area growth can be given as

$$\frac{\partial A_d}{\partial N} = \frac{A^e}{A_{cz}} \frac{\partial A}{\partial N} \tag{3.17}$$

The damage variable growth as function of number of cycles can be derived by substituting eq. 3.14 and eq. 3.16 into eq. 3.13. Thus one get,

$$\frac{\partial d}{\partial N} = \frac{1}{A_{cz}} \frac{\left[\Delta^f (1-d) + d\Delta^0\right]^2}{\Delta^0 \Delta^f} \frac{\partial A}{\partial N} \tag{3.18}$$

The area of cohesive zone is given by Rice as

$$A_{cz} = b \frac{9\pi}{32} \frac{E_3 G^{max}}{(\tau^0)^2} \tag{3.19}$$

where b is width of delamination, E_3 is the Young's modulus in direction perpendicular to crack plane and G^{max} is the maximum energy release rate in a given loading cycle. However, this equation is valid for mode I only. The modified equation proposed by Hallet and Harper [6] and Naghipour *et.al.* [36] is as follows

$$A_{cz,I} = bE_m \frac{G_{Ic}}{(\tau_n^0)^2} \tag{3.20}$$

$$A_{cz,II} = bE_m \frac{G_{IIc}}{(\tau_s^0)^2} \tag{3.21}$$

$$A_{cz,mixed} = scaling factor \times \left[min\left(A_{cz,I}, A_{cz,II}\right)\right] \tag{3.22}$$

The scaling factor in these equations is experimental value and is generally chosen around 0.5. The last term of eq. 3.18 comes from the experimental curve fit and it is given by eq 3.9. It is valid for $G_{th} < G^{max} < G_c$. Otherwise the value of this term is zero. The maximum energy release rate in a cycle is given as

$$G^{max} = \frac{\tau^0}{2} \left[\Delta^0 + \frac{\left(\Delta^f - \lambda^{max} \right)^2}{\Delta^f - \Delta^0} \right] \tag{3.23}$$

Further the value of ΔG is defined as

$$\Delta G = \Delta^{max} - \Delta^{min} \tag{3.24}$$

where the load ratio R is defined as

$$R^2 = \frac{G^{min}}{G^{max}} \tag{3.25}$$

Thus combining eqs 3.23, 3.24 and 3.25, one gets

$$\Delta G = \frac{\tau^0}{2} \left[\Delta^0 + \frac{\left(\Delta^f - \lambda^{max} \right)^2}{\Delta^f - \Delta^0} \right] \left(1 - R^2 \right) \tag{3.26}$$

Thus the formulation described above can take into account the varying load ratio. Thus all the terms needed for implementation of cohesive zone model in case of fatigue load are defined.

3.4 Implementation of cohesive zone model in FEA

The cohesive zone model can be implemented in FEA code either by interface element or by contact elements. Interface elements are the zero thickness elements that are present between the delaminating surfaces. While the contact elements require contact and target surfaces to be defined. In contact elements, the separation is visualised by actual debonding between the surfaces. But the contact search algorithms implemented in FEA are complicated and thus the solution takes longer time for convergence. Therefore the formulation based on interface element is preferred whenever possible.

In this study, the standard interface element with 8 nodes is used. The geometry of single element is as shown the diagram below. The constitutive relation for this element in Voigt notation is given as
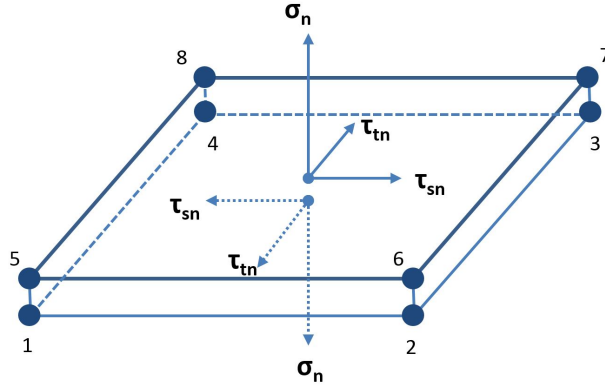

Figure 3.4: 8 noded interface element

$$
\begin{bmatrix} \tau_1 \\ \tau_2 \\ \tau_3 \end{bmatrix} = (1-d)\,K \begin{bmatrix} \Delta_1 \\ \Delta_2 \\ \Delta_3 \end{bmatrix} + dK \begin{bmatrix} \langle -\Delta_1 \rangle \\ 0 \\ 0 \end{bmatrix} \tag{3.27}
$$

As it can be seen from the equation, the negative values of Δ_1 are neglected as it does not affect the delamination process. The damage variable 'd' is used as state variable and is updated at each load step. The formulation is implemented in Matlab. The properties for the cohesive zone are defined as below:

Material property	value
G_{Ic}	$0.075\ kJ/m^2$
G_{IIc}	$0.547\ kJ/m^2$
τ_1^0	61 MPa
$\tau_2^0 = \tau_3^0$	68 MPa
K	$10^6 N/mm^3$
η	1.45

Table 3.1: Properties of cohesive zone [8]

3.4.1 Quasi static loading case

The quasi static loading case is first checked. In Matlab, the formulation is checked for single integration point. The mixed mode load is applied in terms of displacement. 0.005 mm normal separation and 0.003 mm shear separation is applied. For the above properties, the mixed mode onset as defined by eq. 3.8 is $\Delta^0 = 6.2 \times 10^{-5}$ mm. Similarly the mixed mode propagation criteria as per eq. 3.5 is $\Delta^f = 0.0046$ mm.
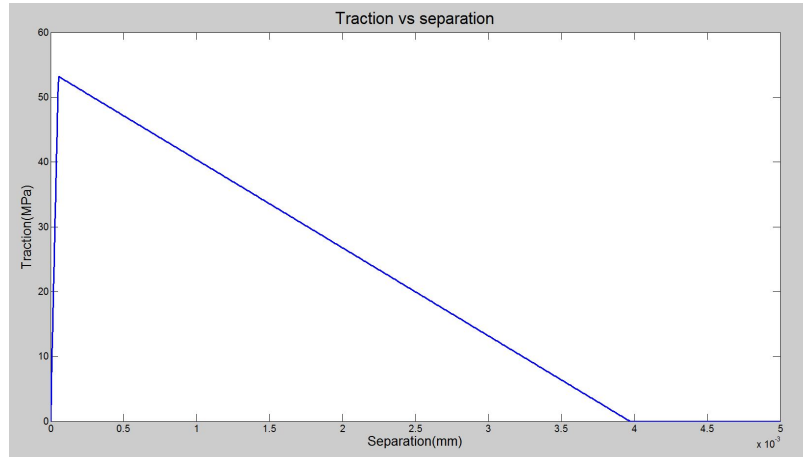

Figure 3.5: Traction-Separation curve

The resultant traction-separation curve is shown in the fig. 3.5 and the growth of damage variable 'd'
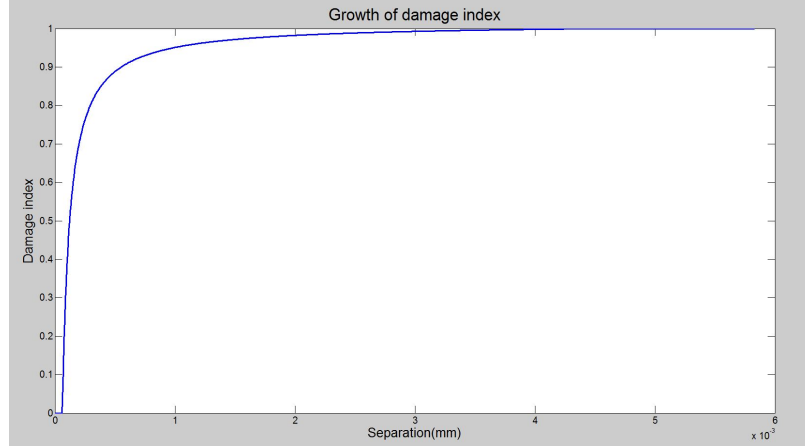
Figure 3.6: Growth of damage variable

is shown in the fig 3.6. From the graphs , one can see that damage onset occurs at very early stage of loading which is the result of high initial stiffness. Once the maximum traction value is reached, the damage index starts to increase as it can be seen in fig 3.6. Once the damage index starts increasing, one can see a linear reduction in the value of traction. This is the softening behaviour of cohesive zone law. Once the damage index reaches zero, it cannot take any load and traction reduces to zero. All this behaviour is correctly captured by the current model.

3.4.2 Fatigue loading case

In case of fatigue loading, the Paris law constants C and m needs to be defined. These values are chosen as $C = 9.59 \times 10^{-6} mm^2$ and $m = 5.5$. [34]. The loading is done in two stages. First the static load is applied in terms of displacements. Typically 0.0015 mm normal separation and 0.003 mm shear separation is applied. This load is kept constant for each cycle and they introduce some initial damage. However, load being below the propagation criteria, the interface does not fail completely. This can be verified from traction-separation graph for the first cycle as shown in fig. 3.7.
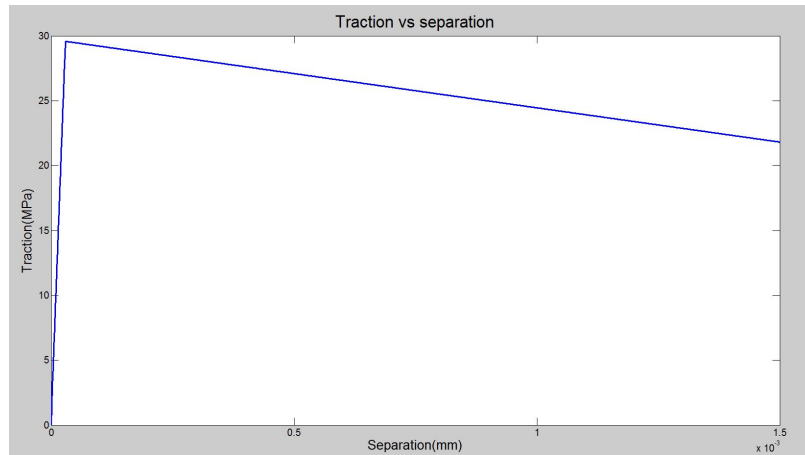
Figure 3.7: Traction-separation curve for first cycle

In second stage, the fatigue damage introduced as defined in eq.3.18. The damage variable starts

24

degrading as the number of cycles are increased. As the fatigue cycles go on increasing, at some point the damage state reaches 1 and the interface fails completely. During this stage, the traction decrease continuously till it reaches zero.
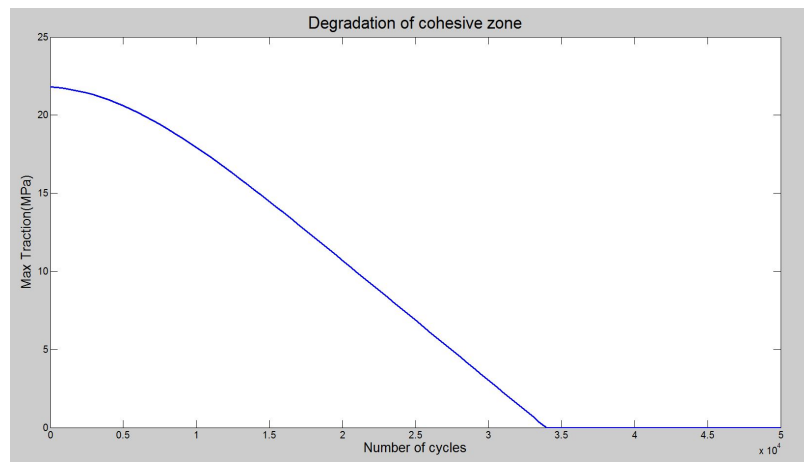
Figure 3.8: Reduction of traction because of fatigue loading

As it can be seen from the fig. 3.8, the value of traction drops to zero around 35000 cycles.

3.4.3 Implementation of cohesive law for quasi static loading case in FEA

Figure 3.9 shows the problem implemented in FEA software package ANSYS. The solid elements used in this case are 8 noded SOLID185. These elements are separated by the interface element INTER205. It is a zero thickness element with 8 nodes. The cohesive zone model described in previous sections is implemented through user programmable subroutine function.
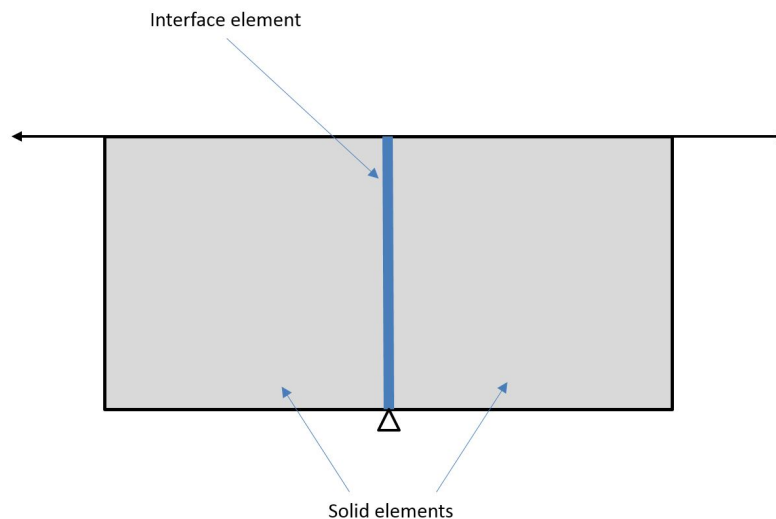
Figure 3.9: Schematics of loading case implemented in FEA

The size of one solid element is 0.5×0.5×0.5 mm. The properties for cohesive element are given according to table 3.1. Only change is that initial stiffness value given is 1000 MPa/mm. Both the
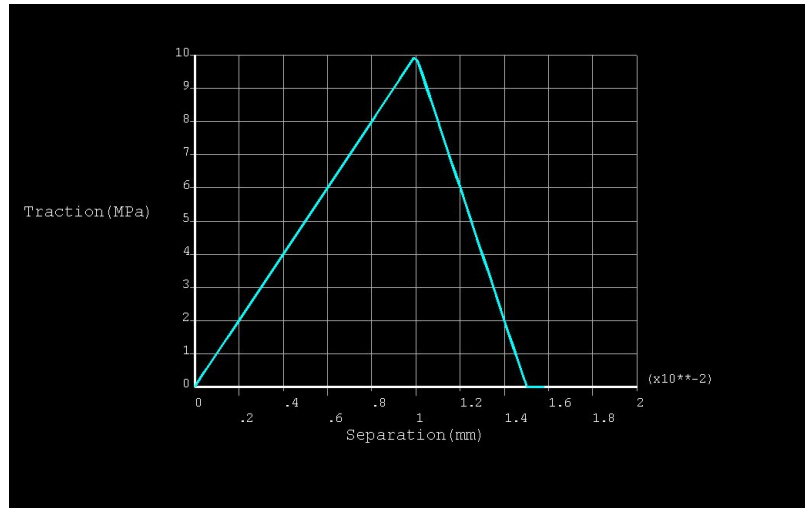
Figure 3.10: Traction vs separation plot

elements are fixed at bottom contact points and load is applied on opposite nodes.

Figure 3.10 shows the traction-separation plot obtained for the interface element. The plot shows the correct trend for the curve as the formulation implemented here is bilinear law. However, due to use of low initial stiffness, the ratio of onset displacement to final displacement is high. Figure
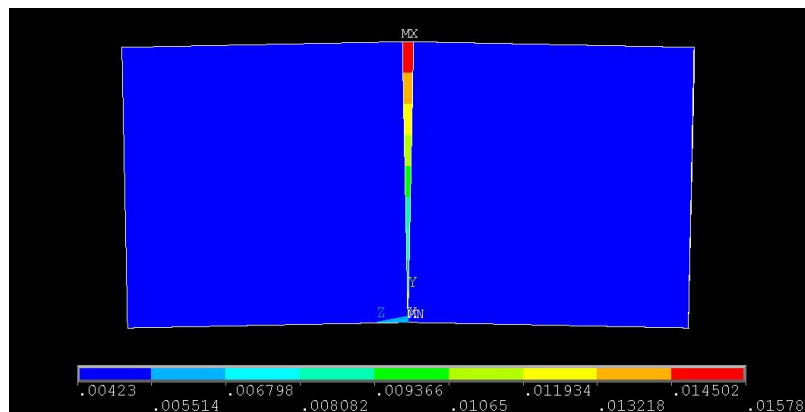
Figure 3.11: separation plot for interface element

3.11 shows the separation caused inside interface element. This trend is predicted correctly as the separation should keep increasing from the pivot point.

3.5 Experimental Determination of interlaminar fracture toughness of GFRP laminates

For implementing any delamination model, the critical energy release rate values (G_{Ic}, G_{IIc} and G_{IIIc}) are needed. These are known as interlaminar fracture toughness. These values are important as most of the cohesive zone models make use of these property. Furthermore, a measurement of interlaminar fracture toughness that is independent of specimen geometry or the force introduction

is useful for establishing design allowables. In this section, the experimental method is discussed for characterization of mode I and mode II interlaminar fracture toughness.

3.5.1 DCB test for mode-I characterization

Mode I is the loading mode in which crack plane is perpendicular to the applied load. The standard used for mode I interlaminar fracture toughness is ASTM D5528 [41]. The standard specimen used for this test is double cantilever specimen loaded at both ends. The specimen geometry, dimensions, and testing parameters are discussed below.

Specimen dimensions
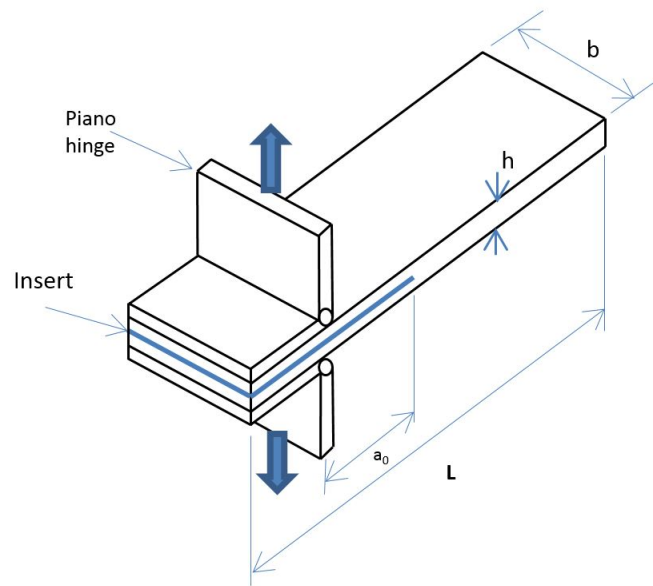
Figure 3.12: Schematic of DCB specimen for G_{Ic} test

Figure 3.12 shows the DCB specimen used in this test. The specimen is made from SIKA glass fiber. The matrix used is mixture of resin CY230 and hardener HY951 in the ratio 10:1. The laminate is unidirectional with all fibers running along length direction. Overall 12 fiber layers are used. The nonadhesive insert is inserted after 6 layers from 1 side of the specimen. Vacuum Assisted Resin Infusion Molding (VARIM) is used for preparation of specimen. Dimensions of the specimen are mentioned in table 3.2.

For loading purpose, hinges are pasted at the delaminated end of specimen. Araldite 2011 adhesive is used for pasting the hinges. The hinge length is 10 mm giving the effective initial delamination length of 40 mm. Both the sides of specimen are painted with white colour which aids in the visual inspection of crack growth.

Experimental parameters deduction

The experiment is carried out on 10 kN Instron machine. The hinges are fixed in the loading fixture and tensile load is applied in displacement control mode. The load is applied at rate of 2.5 mm/min.

Length(L)	128 mm
Width(b)	25 mm
Thickness(h)	3.5 mm
Insert length	50 mm
Insert thickness	40 micron
Initial delamination length (a_0)	40 mm

<div align="center">Table 3.2: Dimensions for DCB specimen</div>
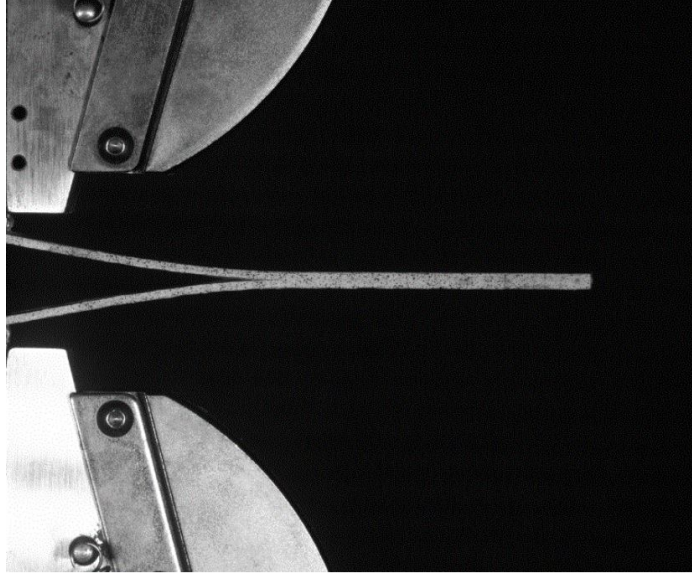
<div align="center">Figure 3.13: Experimental image of DCB specimen being loaded</div>

Load and displacement data is captured continuously. Overall 3 specimen are tested by this method. Figure 3.13 shows the experimental image of DCB specimen.

Calculations and results

Figure 3.14 shows the load-displacement obtained for three DCB specimens tested. After reaching the maximum value, the delamination starts to grow and thus the load curve starts dropping. For calculating the fracture toughness G_{Ic}, three methods are mentioned in the standard based on the data available. They are as follows
1) Modified Beam Theory (MBT) method
2) Compliance Calibration (CC) method
3) Modified Compliance Calibration (MCC) method

In this study, the MBT method is used. The beam theory expression for the strain energy release rate of a perfectly built in double cantilever beam is as follows:

$$G_I = \frac{3P\delta}{2ba} \tag{3.28}$$
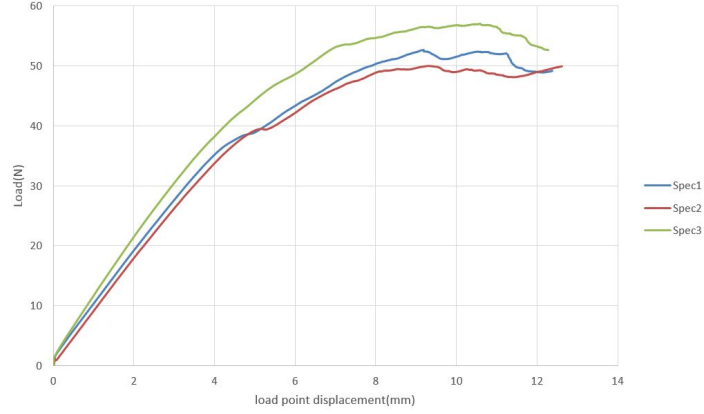
Figure 3.14: Load vs load point displacement graph for DCB specimens

where,

P = load

δ = load point displacement

b = specimen width

a = delamination length

The table below shows the maximum load and maximum displacement obtained for each test specimen. These values are substituted in eq 3.27 to get the final value of G_{Ic}.

Specimen	P_{max} (N)	δ_{max} (mm)	G_{Ic} kJ/m^2
1	52.7089	9.1868	0.5811
2	50.0682	9.2822	0.5577
3	57.008	10.5906	0.7245
Average	53.2617	9.6865	0.6211

Table 3.3: Experimental results for DCB test

Thus the experimentally calculated interlaminar fracture toughness for mode I is 0.6211 kJ/m^2 or 0.6211 N/mm.

3.5.2 ENF test for mode-II characterization

Mode II loading is the one in which crack plane is parallel to the load and crack propagates in the direction of load. The standard used for mode II interlaminar fracture toughness evaluation is ASTM D7905 [42]. The specimen recommended for this test is the End Notched Flexure (ENF) specimen. This test can be performed with 3 point bending or 4 point bending fixture. But the formulation for 4 point bending test is still being developed. Thus in this study, only 3 point bending test is discussed. The specimen geometry, dimensions and experimental results are discussed below.

Figure 3.15: Schematic of ENF specimen for G_{IIc} test

Specimen dimensions

Figure 3.15 shows the typical specimen required for ENF test. Just like DCB specimen, this is also made from SIKA Glass fiber and matrix made from mixture of CY230 and HY951in ratio 10:1. The laminate consists of 12 layers. nonadhesive insert is placed after 6 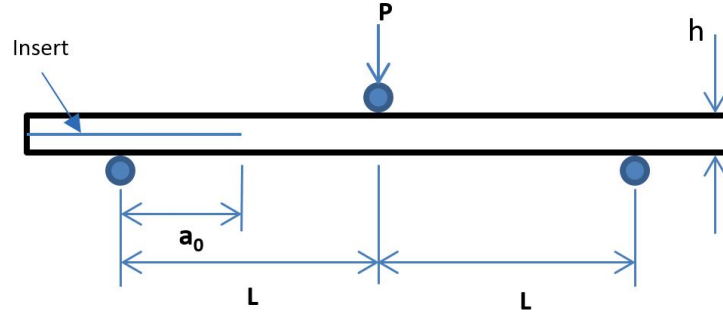layers to simulate the initial delamination. Specimen is prepared by VARIM method. Dimensions of specimen are mentioned below.

Overall length	128 mm
Distance between rollers($2L$)	100 mm
Width(b)	25 mm
Thickness(h)	3.5 mm
Insert length	50 mm
Insert thickness	40 micron

Table 3.4: Dimensions of ENF specimen

Experimental parameter deduction

The experiment is carried out on 100 kN MTS servo hydraulic cyclic test machine. Specimen is fixed in three point bending fixture so as shown in the fig 3.16. The load is applied in displacement control mode at 0.5 mm/min as mentioned in the standard. Both sides of specimen are coated with white paint to visualize the crack growth.

The test is carried out in two stages. In stage one, the specimen is tested without precrack and in stage two, same specimen with the precrack is tested. Initially the compliance of specimen needs to be found out. Therefore the specimen is fixed such that the delamination length ahead of bottom roller is 20 mm. And load is applied till it reaches 250 N. This final value should not exceed the half of maximum load carried by specimen. The load-displacement is then recorded from MTS equipment. Same procedure is again repeated for a test specimen containing delamination length of
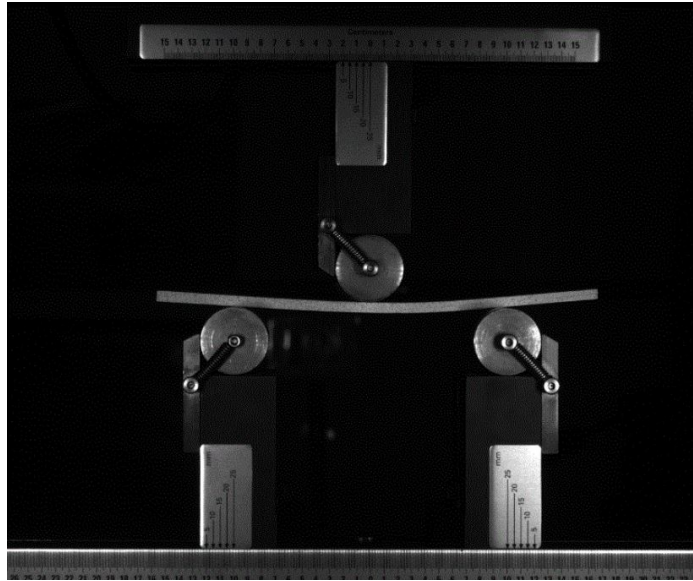
Figure 3.16: Experimental image of ENF specimen being loaded

40 mm. Again load-displacement data is captured. Now the specimen is fixed for initial delamination length of 30 mm. The loading is then continued till the crack starts to grow. At this point, one can see the reduction in load. In stage two, the specimen is removed from fixture and new position of delamination front is marked. Again same procedure carried out in stage 1 is followed with crack lengths of 20 mm, 40 mm, 30 mm.

Calculations and results
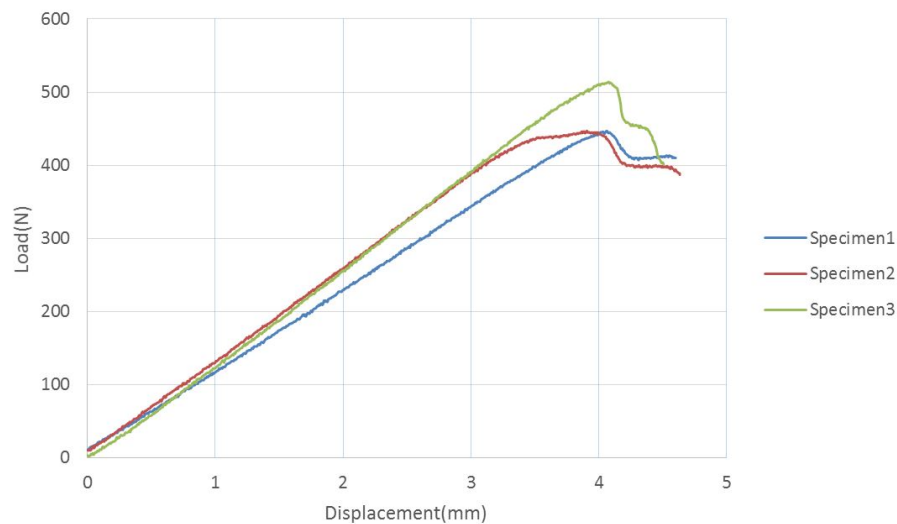
Figure 3.17: Load vs displacement graph obtained for ENF specimens

Figure 3.17 shows the plot of load vs displacement obtained in case of ENF specimen. It can be seen that the load drops at the point when crack starts to propagate. Then one has to plot the

31

graph of compliance vs cube of crack length. The stiffness of each specimen can be found from the load-displacement curve. By fitting the linear equation to the curves of fig 3.18, stiffness of the
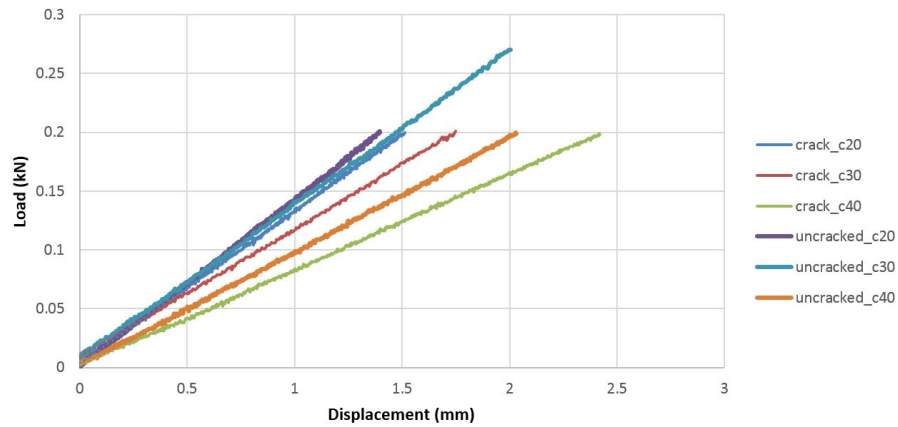
Figure 3.18: Load vs displacement graph for ENF specimen 1

specimen is sfound. The compliance can be found out by reciprocal of stiffness. Thus now we have 6 values of compliance for 6 values of crack length. Now we fit a curve for equation below:

$$C = A + ma^3 \tag{3.29}$$

Here, C and m are known as compliance calibration coefficients. Using the six values obtained from testing, the curve is fitted as shown in the fig 3.19. While plotting this curve, one has to exclude any initial nonlinearity if present.
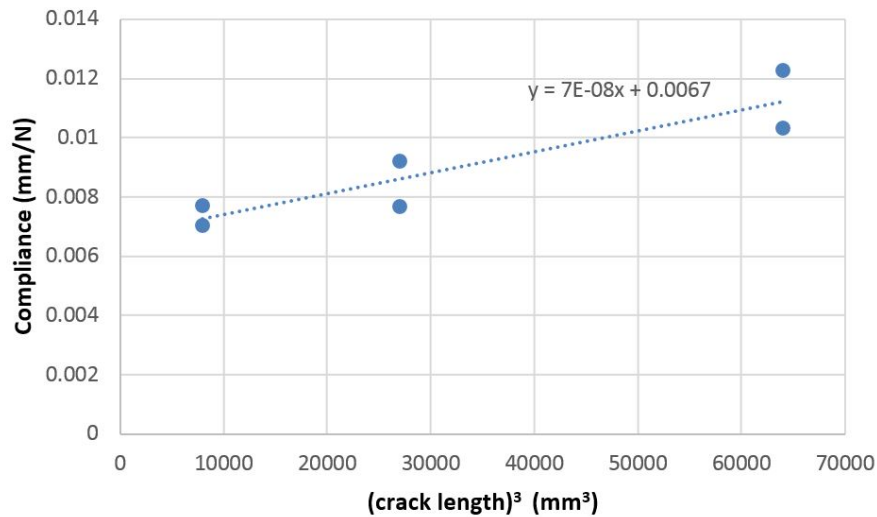
Figure 3.19: Compliance vs a^3 graph for ENF specimen1

The values of compliance calibration coefficients are obtained as $A = 0.0067$ and $m = 7 \times 10^{-8}$.

As mentioned in standard, the fracture toughness value is estimated using the following equation

$$G_{IIc} = \frac{3mP_{max}^2 a_0^2}{2B} \tag{3.30}$$

where, m is the compliance calibration coefficient, P_{max} is the maximum force taken by specimen, a_0 is initial crack length measured from roller and B is the specimen width. The results obtained for three tests are summarised in the table 3.5 given below.

Specimen	P_{max} (N)	m	A	G_{IIc} kJ/m^2
1	479	7×10^{-8}	0.0067	0.867
2	469.5	7×10^{-8}	0.0061	0.833
3	493	6×10^{-8}	0.0063	0.787
Average	480.5			0.829

Table 3.5: Experimental results for ENF test

Thus, experimentally determined value of G_{IIc} for GFRP laminate is 0.829 kJ/m^2 or 0.829 N/mm.

3.6 Closure

The cohesive zone model delamination prediction is presented in this chapter. This model is derived for the mixed mode delamination in case of quasi static loading. Later the fatigue damage is introduced in the formulation. The delamination growth under fatigue loading is implemented by making use of Paris law. Initially the formulation is implemented in Matlab for a single gauss point and it shows the correct trend for quasi static as well as fatigue delamination. The formulation is also implemented in FEA using interface element. But there is problem of convergence owing to the very high initial stiffness. Thus the results presented here are obtained by reducing the initial stiffness. This results in high ratio of onset separation to final separation. Thus the model presented in this study needs to be refined. In this formulation, the governing parameters for bilinear cohesive zone model are critical fracture toughness (G_c), maximum traction (τ_{max}) and initial stiffness (K). However, this may not be the correct way to govern the cohesive law. Instead of initial stiffness, the ratio of onset separation to final separation (Δ_0/Δ_f) would be a more effective parameter. Finally the experimental characterization is done for interlaminar fracture toughness for GFRP specimen for mode-I and mode-II. The values of G_{IC} and G_{IIC} are obtained from tests as per ASTM standards and they are 0.621 kJ/m^2 and 0.829 kJ/m^2 respectively.

Chapter 4

Infrared non destructive assessment of delamination growth in composite laminates under cyclic loads

4.1 Introduction

In this chapter, the infrared non destructive testing(IRNDT) method is presented. Infrared thermography is a fast and full field analysis technique that is capable of in-situ damage assessment. This method makes use of the thermal properties of material to detect the damage present inside the laminate. The damage generated in the laminate alters the thermal conductivity of the damaged region locally. Therefore the images captured using the infrared camera shows local colder spots. These colder spots can be related to the subsurface damage present inside the laminate. Figure 4.1 shows the schematic of IRNDT.
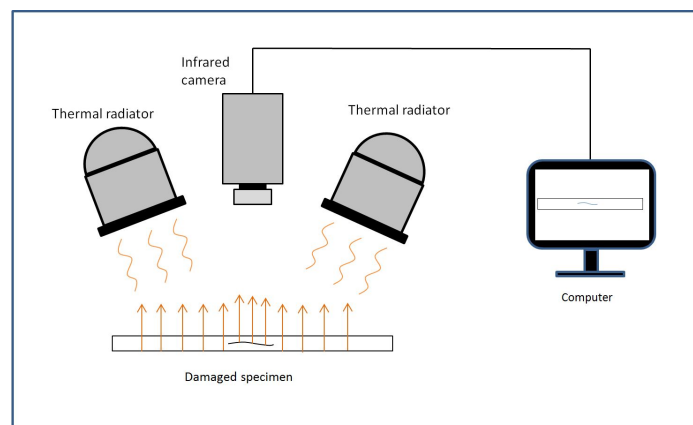

Figure 4.1: Principle of Infrared Non Destructive Testing

Various types of damages occur inside composite materials as explained previously. These damages may be at surface or may occur inside the laminate. The damages that occur on the surface are very easy to visualize. But the damages occurring inside the laminate are hard to track. Various methods are available to track the internal damage occurring in composites. Some of them are X-ray Computed Tomography, Infrared Thermography, Acoustic emission etc. The method used in this work is IRNDT.

IRNDT makes use of the thermal properties of materials. Heat conductivity of the specimen is used to track the damage development inside the laminate. The specimen is first heated with light/heat source. The heat is absorbed inside the specimen and is reflected back to the surface. Then the image is captured using infrared camera. The infrared camera can easily pick up the temperature variation. This temperature variation can be directly related to the damage present in the component.

4.2 Experimental Specimen preparation

Experimental specimen are prepared using vacuum assisted resin infusion molding(VARIM). The layup sequence chosen for this study is $[45/0/-45/90]_s$. The composite laminates are made from SIKA glass fiber material. The matrix is made from resin CY230 and hardener HY951. The mixing ratio of resin to hardener is 10:1 by weight. The advantage of using above mentioned resin hardener combination is low viscosity of resin. This property helps in the infusion of resin happen smoothly. Figure 4.2 shows the images in sequence in the case of VARIM process.

As the figure 4.2a shows the layers are stacked above each other. The layer sequence from bottom is mylar sheet, fibers, perforated sheet, peel ply and green mesh. The spiral pipes for input and suction of resin are placed at opposite ends of casting. Then the whole assembly is covered by vacuum bag and sealed at edges using sealing tape. Then the suction side pipe is clamped and vacuum pump is started. This ensures the perfect sealing if vacuum pressure remains constant. The maximum vacuum created is -96 kPa. If the pressure increases after disconnecting the pump, the whole casting area is checked for leakages. Once the perfect vacuum condition is achieved, the vacuum pressure is reduced to -20 kPa so that resin transfer will occur slowly and all fibers will get wet with resin. Once the resin transfer process is complete, the vacuum pressure is increased again to full capacity so as to remove the air trapped in between the layers. This air along with extra resin is sucked towards the suction side (see fig. 4.2d) where is collected in a catch pot. Once the infusion process is complete, both the input and suction lines are clamped. The casting is then kept at same condition for curing tocomplete for 24 hours.

For the experiment mentioned in this work, laminate of size 300×300 mm^2 is made using VARIM process. The specimen of size 250×25 mm^2 are then machined from the laminate. The edges of specimen are ground using fine grit sandpaper to remove any edge imperfections and loose fibers which result from the machining process. For the specimen with hole, a 5 mm diameter hole is used. The hole is drilled at the center of specimen. Wooden backing plate is used for drilling to prevent the damage development near hole. Then tabs are pasted at the gripping point of specimen to evenly distribute the gripping pressure over the tab area. Tabs are made from Aluminium and have a dimension of 50×25 mm^2. The inner side of tabs are chamfered at an angle of 45°. The two part adhesive used for bonding tabs is done with Araldite AV138 and hardener HV998 mixed in the ratio of 10:4. The specimen prepared by this method have very high fiber volume fraction as well
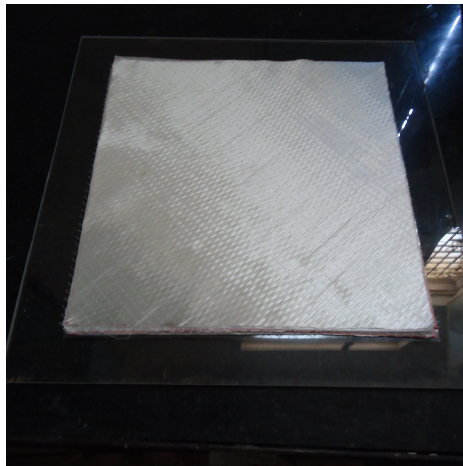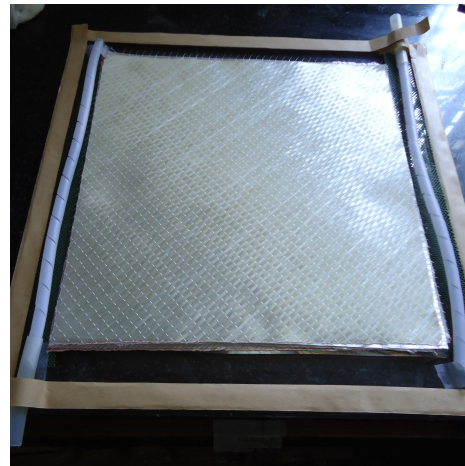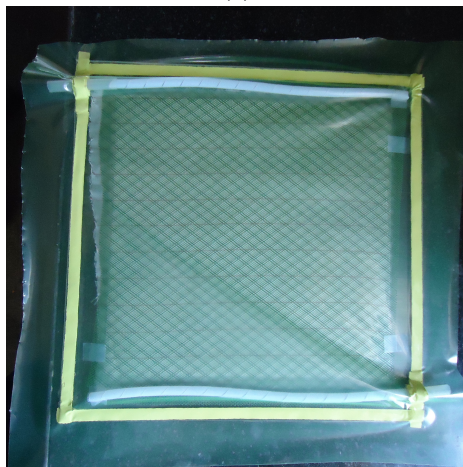
Figure 4.2: Manufacturing of glass fiber composite specimen using Vacuum Assisted Resin Infusion process: a)layup of fibers, b)attaching pipes and sealing tape, c)laying up vacuum bag, d)applying vacuum and suction of resin, e)final laminate, f)machined specimen

as weight fraction. This reduces the irregularities in thickness as in case of in the process of hand layup technique.

4.3 Interrupted fatigue testing of GFRP specimen without hole and with hole

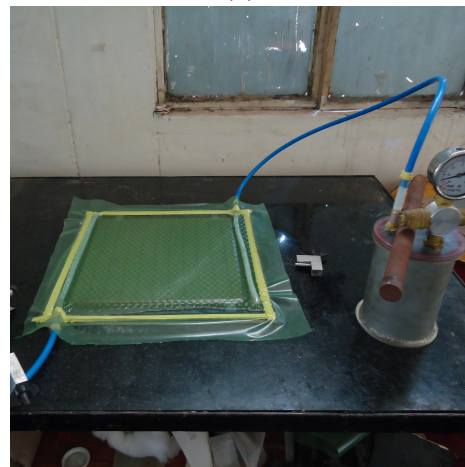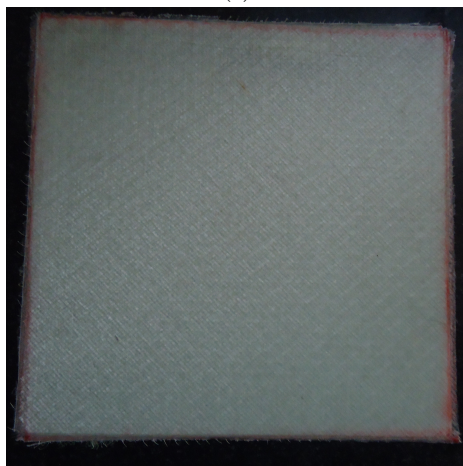The interrupted fatigue testing is carried out on the GFRP specimen. The testing is carried out on MTS servo hydraulic cyclic test machine of 100 kN capacity. The test is performed on the specimen with and without hole. The specimen gripping pressure is kept at 900 psi. A constant amplitude fatigue load is applied at 5 Hz with maximum and minimum loads of 8 kN and 0.8 kN respectively. For the static testing of specimen an extensometer with a gauge length of 20 mm is used for axial strain measurement.

(a) without hole   (b) with hole
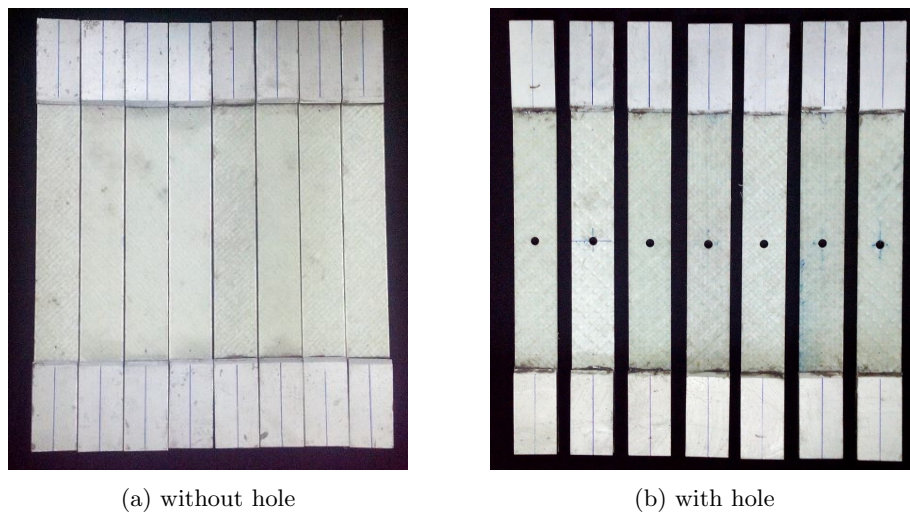
Figure 4.3: Specimen considered for experimental work

4.3.1 Fatigue testing of specimen without hole

Before conducting the fatigue testing, it is important to know the initial strength and stiffness of the specimen being considered. Therefore quasi static testing is carried out at beginning to find the strength and stiffness of the specimen. Figure 4.4 shows the stress vs strain graph of virgin GFRP specimen. Using this data, the initial stiffness and strength of specimen is found out and summarised in table 4.1 as shown below:

As it can be seen from table 4.1 the average strength of specimen is 302.61 MPa and average modulus is 194.1 MPa. Based on this data the fatigue load amplitude can be estimated. The fatigue load amplitude chosen is 130 MPa and the load ratio is kept as 0.1. Further tension tension cycle is chosen. The fatigue life of specimen is later found out by testing the specimen under cyclic loading till the failure. It is found to be 8400 cycles. Then the tests are repeated for 1000, 3000, 5000 and 7000 cycles. As the specimen haven't reached their fatigue life, the specimen will not fail. For each number of cycles, two specimens are tested. Later, a quasi-static test is performed on those specimen to predict the residual stiffness and residual strength respectively.
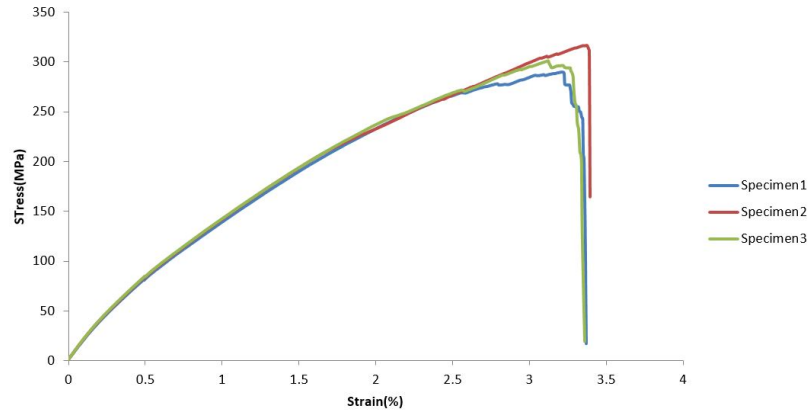
Figure 4.4: Stress vs strain curve for unfatigued specimen

Specimen	Stiffness MPa	Strength MPa
1	190.8	290.17
2	194.49	316.26
3	197	301.4
Average	194.1	302.61

Table 4.1: Strength and stiffness of unfatigued specimen
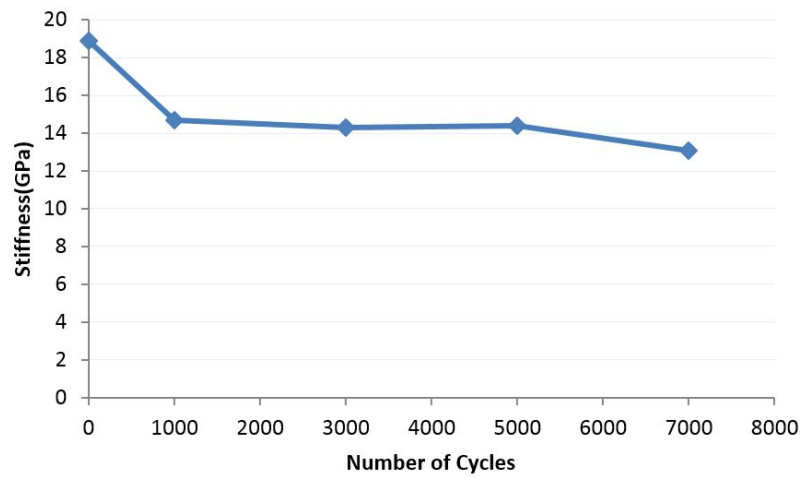
Figure 4.5: Residual stiffness variation with number of cycles

Figure 4.5 and 4.6 show the variation of stiffness and strength degradation of specimen without hole. The stiffness of specimen remains almost constant after the initial degradation. However, severe drop in the strength of component is observed. In literatures, it is mentioned that the stiffness should remain almost constant. But during the first loading cycle, some damage is introduced in laminate. Therefore, experimentally initial drop is expected to account for the damage generated.
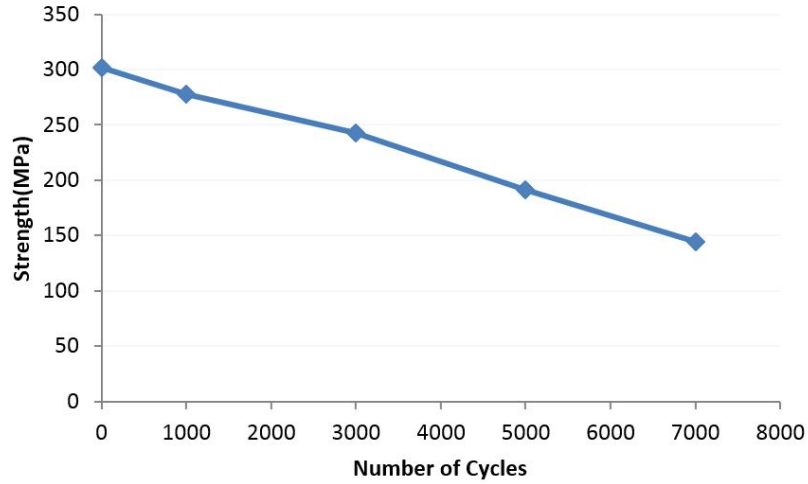
Figure 4.6: Residual strength variation with number of cycles

Thereafter, it remains unchanged.

4.3.2 Fatigue testing of specimen with hole
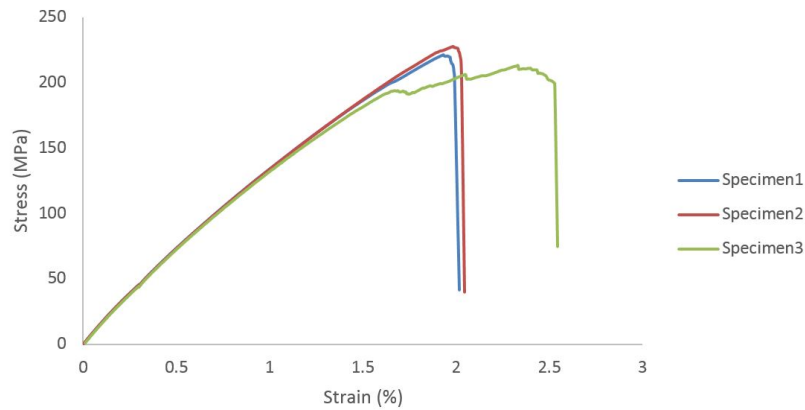
Figure 4.7: Stress vs strain curve for virgin GFRP specimen

Plate with hole introduces the stress concentration near hole periphery. And it increases the severity of damage around the hole with increasing fatigue cycle. Most of the composite structures have holes in them. Thus it is important to study the fatigue properties of GFRP specimen with hole. Later similar testing of plate without hole is carried out for these specimens under similar conditions and loading. First the specimen are tested quasi statically to find the strength and stiffness of virgin specimen. Three specimen are tested and the results are as shown in the table 4.2 below. As shown in the table 4.2, the average strength of specimen is 222.58 MPa and the average modulus is 15.52 GPa. Now the fatigue loads are applied to the specimens. The maximum load in cycle is kept same as the plate without hole sample i.e. 130 MPa. The load ratio is 0.1. First the fatigue life of specimen is found out. It turned out to be 2000 cycles. Then the specimen are tested under

Specimen	Stiffness GPa	Strength MPa
1	15.62	227.47
2	15.53	227.47
3	15.41	212.80
Average	15.52	222.58

Table 4.2: Strength and stiffness of virgin specimen

fatigue loading for 350, 850,1400 and 1900 cycles. The ratio of n/N_f for these intervals is kept same as that of specimen without hole. Quasi static test is then performed on these specimen to get the residual stiffness and residual strength at various stages as defined earlier.

Figure 4.8: Residual stiffness variation with number of cycles

Figure 4.9: Residual strength variation with number of cycles

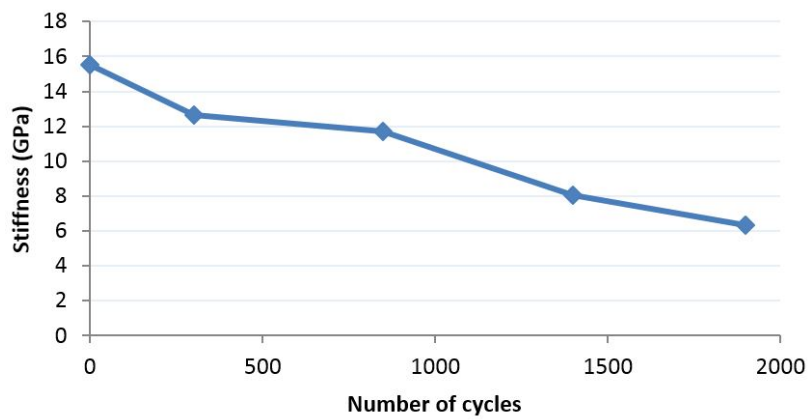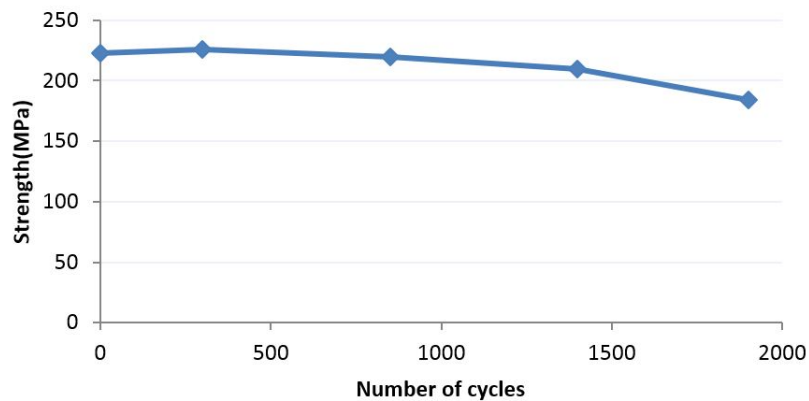As fig 4.8 shows, the stiffness of specimen goes on decreasing with increasing cycle. This behaviour can be expected due to the presence of hole. In case of specimen without hole, the

damage is spread throughout the specimen as there are no stress concentrations present. But in case of specimen with hole, the damage growth is accelerated from the periphery of hole. Thus as number of cycles increase, the drop in stiffness may be expected and it it observed. Figure 4.9 shows the strength variation for same case. Unlike specimen without hole, the stiffness in this case does not vary much.

4.4 Infrared thermography results

The infrared thermography can be effectively used to track the subsurface damage taking place in composites. There are three varients of thermographic analysis widely used. They are pulse thermography, transient thermography, and lock-in thermography. The choice of method depends on the application. The flash thermography makes use of flash lamps for a duration of fraction of seconds. It is used when the thickness of specimen is very small or heat conductivity of material is very good e.g. to detect the corrosion behind the paint or for detecting defects in metals. The transient thermography is for moderately thicker specimen or for materials with low thermal conductivity e.g. in case of composites. This method makes use of more powerful light/heat source like halogen lamps. Thus the details of deeper defects can be outlined. The last method is lock-in thermography. This method is useful for very thick specimen. The stimulus in this case can be halogen lamps, ultrasound or mechanical stimulation as long as it does not affect the properties of material. In this study, composite specimen with a thickness of 2.4 mm is considered. Therefore the most effective method would be transient thermography.
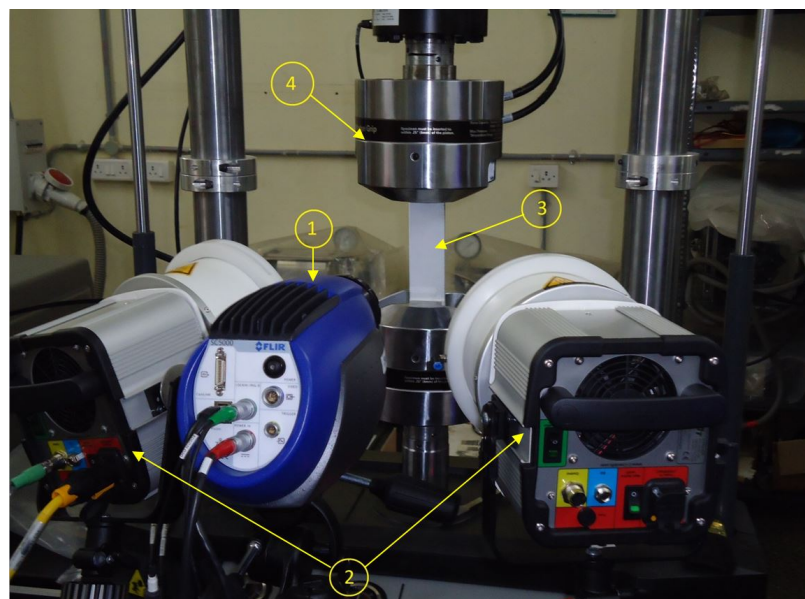
Figure 4.10: Experimental setup for Infrared Non Destructive Testing

Figure 4.10 shows the infrared thermography setup for transient thermography. The infrared camera used is FLIR SC5000. Its resolution is 320×256 at full resolution and sensitivity is 20 mK. The camera is connected to the computer through a BNC cable and triggering signal to camera is given from the computer. The light source used is halogen lamps with a maximum power of 2500

W at 230 V. Both the light sources are synched together. The specimen without hole and with hole under fatigue are inspected using this method. The thermographic inspection is carried out at room temperature of 22^oC. Before starting the test, the camera needs to be focussed sharply over the specimen. Once the focussing is done, the excitation signal is given to camera and halogen lamps and the image capturing the begins. The experimental parameters used for inspection are as follows:

Inspection method	:	Transient thermograpgy
Excitation source	:	Halogen lamps
Modulation	:	Sinus
Max amplitude	:	90%
Duty cycle	:	6 s
Excitation period	:	15 s

(a) n = 0   (b) n = 1000   (c) n = 3000   (d) n = 5000   (e) n = 7000
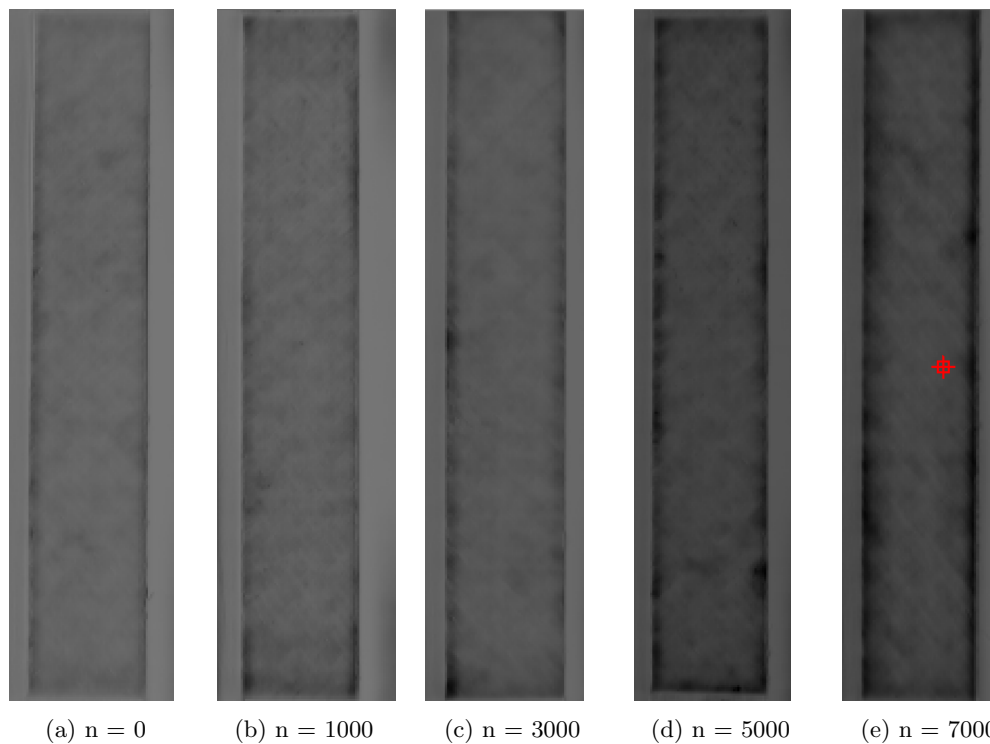
Figure 4.11: Infrared results of specimen without hole obtained in case of fatigued specimen

Duty cycle is the time for which the light source is active and excitation period is the time for which infrared images are captured. Figure 4.11 shows the results of infrared thermography images obtained in case of prefatigued specimen without hole. The images shown are post-processed from software package IrNDT. The black region in specimen indicates the change in thermal conductivity of specimen. This again corresponds to the damage present at that particular point. Thus one can

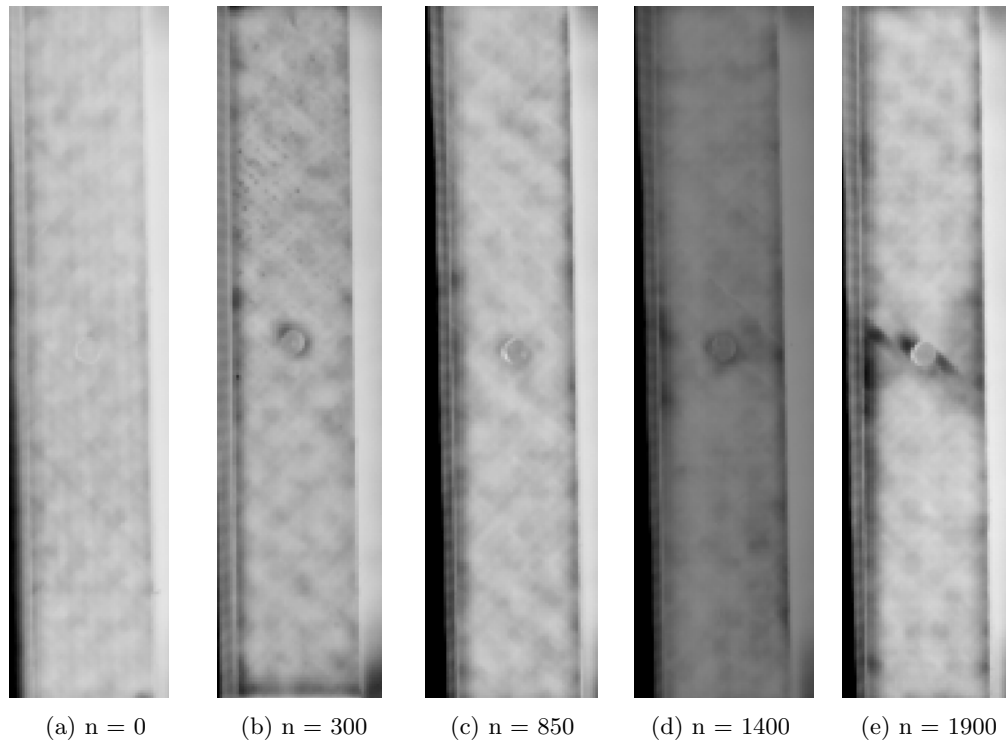(a) n = 0   (b) n = 300   (c) n = 850   (d) n = 1400   (e) n = 1900

Figure 4.12: Infrared images of specimen with hole obtained in case of fatigued specimen

see that in absence of any stress concentration, the damage starts to develop from the stress free outer edges of specimen. This phenomenon is observed by many references in literature [43, 44]. The initial specimen seem to have very small defects near the hole edges. It is due to machining of specimen. However, as the number of cycles go on increasing, the damage can be seen propagating inside the specimen from the edges.

Figure 4.12 shows the infrared images obtained in case of fatigued specimen with hole at various cycles. The test parameters are kept exactly same as those used for specimen without hole. One can observe that the damage grows from outer edge of specimen as well as from the hole periphery. This indicates that an accelerated damage growth in the specimen is observed and results in early failure of the specimens as compared to specimens without hole.

4.5 Closure

The experimental work is carried out to assess fatigue degradation of stiffness and strength in GFRP laminates. The test is carried out on both specimen without hole and other with hole. The test results show a linear degradation of stiffness with increasing cycles after some initial degradation. The strength of specimen also goes on reducing with increasing cycles. The static strength of specimen with hole is 74% of that of specimen without hole. However, the fatigue life of specimen is greatly reduced due the presence of hole. The fatigue life of specimen without hole is 8000 cycles whereas for specimen with hole is 2000 cycles at the same load ratio. The infrared thermography is

employed to assess the damage in the specimen which are fatigued at various fraction of their fatigue life. The damage growth is studied using the transient thermography method. In case of specimen without hole, the damage starts to grow from the edges of specimen and propagates inwards. In case of specimen with hole, the damage starts to grow from edges as well as from the periphery of hole. Due to the presence of stress concentrations the stiffness in these specimen drops much further as compared to the specimen with hole.

Chapter 5

Conclusion and recommendation for future work

5.1   Concluding remarks

In this work, the progressive damage model for composites under fatigue loading is implemented. Later the model is based on gradual stiffness degradation as well as gradual strength degradation. The model is able to predict degradation of both residual strength and residual stiffness of the laminate with the increasing cycle. However, the delamination propagation is not predicted correctly and therefore the cohesive zone model is considered. The cohesive zone law is derived based on bilinear formulation for both quasi static as well as fatigue loading. The behaviour of cohesive zone model is verified in Matlab. Finally, the implementation is done in FEA software ANSYS 15 using interface element. The user programable features are used to write the user defined CZM subroutine. However, high initial stiffness resulted convergence issues.

In the experimental section, the vacuum assisted resin infusion molding (VARIM) is employed for laminate manufacturing. The GFRP specimen are characterized for interlaminar fracture toughness as per ASTM recommended tests. Then tested under constant amplitude fatigue loading. The residual stiffness and strength degrade with increasing cycles and it shows the same trend as reported in literature. The infrared thermography technique is employed to assess the damage growth in composites under fatigue loading. It is able to predict the damage growth correctly and thus can be effectively used for in situ damage evaluation in composite laminate.

5.2   Scope for future work

- The progressive damage model presented in this study makes use of Hashin's failure criteria. However, Hashin's criteria is one of the oldest criteria. Newer failure criteria which are more close to the actual failure phenomenon like LARC04 can be implemented .

- The cohesive zone model needs to be further refined as the problem is arising because of high initial stiffness. The formulation needs to be rederived by for delamination propagation in displacement jump space instead of traction based formulation.

- Viscous regularization may be implemented within user defined cohesive zone to achieve the convergence of solution. It can be used to avoid nonconvergence occurring at the onset of delamination growth.

- The fatigue delamination growth can be experimentally studied to obtain the Paris law curve.

References

[1] C. R. C. EADS Deutschland GmbH. The research requirements of the transport sectors to facilitate an increased usage of composite materials .

[2] T. L. Anderson and T. Anderson. Fracture mechanics: fundamentals and applications. CRC press, 2005.

[3] S. G. Pantelakis and E. C. Kyriakakis. Fatigue damage of APC-2 composite assessed from material degradation and non-destructive evaluation data. *Theoretical and applied fracture mechanics* 32, (1999) 37–46.

[4] M. M. Shokrieh and L. B. Lessard. Progressive fatigue damage modeling of composite materials, Part I: Modeling. *Journal of Composite Materials* 34, (2000) 1056–1080.

[5] Z. Zou, S. Reid, and S. Li. A continuum damage model for delaminations in laminated composites. *Journal of the Mechanics and Physics of Solids* 51, (2003) 333–356.

[6] P. W. Harper and S. R. Hallett. Cohesive zone length in numerical simulations of composite delamination. *Engineering Fracture Mechanics* 75, (2008) 4774–4792.

[7] P. Papanikos, K. Tserpes, and S. Pantelakis. Modelling of fatigue damage progression and life of CFRP laminates. *Fatigue & Fracture of Engineering Materials & Structures* 26, (2003) 37–47.

[8] A. Turon, P. P. Camanho, J. Costa, and C. Dávila. A damage model for the simulation of delamination in advanced composites under variable-mode loading. *Mechanics of Materials* 38, (2006) 1072–1089.

[9] V. V. Vasiliev and E. Morozov. Mechanics and analysis of composite materials. Elsevier, 2001.

[10] S. Selvaraju and S. Ilaiyavel. Applications of composites in marine industry. *J. Eng. Res. Stud.,* II 89–91.

[11] H. Z. Failure Criteria for unidirectional fibre composites. *J.Appl.Mech.* 47, (1980) 329–334.

[12] C. K. Chang FK. A Progressive damage model for laminated composites containing stress concentrations. *Journal of Composite Materials* 21, (1987) 834–855.

[13] K. M. Ubaid J and R. M. Strength prediction and progressive failure analysis of carbon fiber reinforced polymer laminate with multiple interacting holes involving three dimensional finite element analysis and digital image correlation. *International Journal of Damage Mechanics* 23, (2014) 609–635.

[14] S. Khedkar, V. Chinthapenta, M. Madhavan, and M. Ramji. Progressive failure analysis of CFRP laminate with interacting holes under compressive loading. *Journal of Composite Materials* .

[15] M. Kashfuddoja and M. Ramji. Whole-field strain analysis and damage assessment of adhesively bonded patch repair of CFRP laminates using 3D-DIC and FEA. *Composites Part B: Engineering* 53, (2013) 46–61.

[16] M. Kashfuddoja and M. Ramji. Whole-field strain analysis and damage assessment of adhesively bonded patch repair of CFRP laminates using 3D-DIC and FEA. *Composites Part B: Engineering* 53, (2013) 46–61.

[17] H. Z. Fatigue failure criteria for unidirectional fiber composites. *Journal of Applied Mechanics* 48, (1981) 846–852.

[18] M. M. Shokrieh and L. B. Lessard. Progressive fatigue damage modeling of composite materials, Part II: Material characterization and model verification. *Journal of Composite Materials* 34, (2000) 1081–1116.

[19] K. Tserpes, P. Papanikos, and T. Kermanidis. A three-dimensional progressive damage model for bolted joints in composite laminates subjected to tensile loading. *Fatigue & Fracture of Engineering Materials & Structures* 24, (2001) 663–675.

[20] L. Ye. Role of matrix resin in delamination onset and growth in composites. *Composites science and technology* 33, (1988) 257–277.

[21] W. Van Paepegem, J. Degrieck, and P. De Baets. Finite element approach for modelling fatigue damage in fibre-reinforced composite materials. *Composites Part B: Engineering* 32, (2001) 575–588.

[22] J. R. Rice. A path independent integral and the approximate analysis of strain concentration by notches and cracks. *Journal of applied mechanics* 35, (1968) 379–386.

[23] D. Dugdale. Yielding of steel sheets containing slits. *Journal of the Mechanics and Physics of Solids* 8, (1960) 100–104.

[24] G. I. Barenblatt. The mathematical theory of equilibrium cracks in brittle fracture. *Advances in applied mechanics* 7, (1962) 55–129.

[25] A. Hillerborg, M. Modéer, and P.-E. Petersson. Analysis of crack formation and crack growth in concrete by means of fracture mechanics and finite elements. *Cement and concrete research* 6, (1976) 773–781.

[26] V. Tvergaard and J. W. Hutchinson. The relation between crack growth resistance and fracture process parameters in elastic-plastic solids. *Journal of the Mechanics and Physics of Solids* 40, (1992) 1377–1397.

[27] A. Needleman. A continuum model for void nucleation by inclusion debonding. *Journal of applied mechanics* 54, (1987) 525–531.

[28] X.-P. Xu and A. Needleman. Numerical simulations of fast crack growth in brittle solids. *Journal of the Mechanics and Physics of Solids* 42, (1994) 1397–1434.

[29] Y. Mi, M. Crisfield, G. Davies, and H. Hellweg. Progressive delamination using interface elements. *Journal of composite materials* 32, (1998) 1246–1272.

[30] C. G. Dávila, P. P. Camanho, and A. Turon. Effective simulation of delamination in aeronautical structures using shells and cohesive elements. *Journal of Aircraft* 45, (2008) 663–672.

[31] P. P. Camanho, C. Davila, and M. De Moura. Numerical simulation of mixed-mode progressive delamination in composite materials. *Journal of composite materials* 37, (2003) 1415–1438.

[32] J. Munoz, U. Galvanetto, and P. Robinson. On the numerical simulation of fatigue driven delamination with interface elements. *International journal of fatigue* 28, (2006) 1136–1146.

[33] R. Peerlings, W. Brekelmans, R. De Borst, and M. Geers. Gradient-enhanced damage modelling of high-cycle fatigue. *International Journal for Numerical Methods in Engineering* 49, (2000) 1547–1569.

[34] A. Turon, J. Costa, P. Camanho, and C. Dávila. Simulation of delamination in composites under high-cycle fatigue. *Composites Part A: applied science and manufacturing* 38, (2007) 2270–2282.

[35] P. Robinson, U. Galvanetto, D. Tumino, G. Bellucci, and D. Violeau. Numerical simulation of fatigue-driven delamination using interface elements. *International journal for numerical methods in engineering* 63, (2005) 1824–1848.

[36] P. Naghipour, M. Bartsch, and H. Voggenreiter. Simulation and experimental validation of mixed mode delamination in multidirectional CF/PEEK laminates under fatigue loading. *International Journal of Solids and Structures* 48, (2011) 1070–1081.

[37] L. B. Lessard and M. M. Shokrieh. Two-dimensional modeling of composite pinned-joint failure. *Journal of Composite Materials* 29, (1995) 671–697.

[38] F.-K. Chang and K.-Y. Chang. Post-failure analysis of bolted composite joints in tension or shear-out mode failure. *Journal of Composite Materials* 21, (1987) 809–833.

[39] C. McCarthy, M. McCarthy, and V. Lawlor. Progressive damage analysis of multi-bolt composite joints with variable bolt–hole clearances. *Composites Part B: Engineering* 36, (2005) 290–305.

[40] M. Benzeggagh and M. Kenane. Measurement of mixed-mode delamination fracture toughness of unidirectional glass/epoxy composites with mixed-mode bending apparatus. *Composites science and technology* 56, (1996) 439–449.

[41] Standard Test Method for Mode I Interlaminar Fracture Toughness of Unidirectional Fiber-Reinforced Polymer Matrix Composites ASTM D5528–01.

[42] Standard Test Method for Determination of the Mode II Interlaminar Fracture Toughness of Unidirectional Fiber-Reinforced Polymer Matrix Composites ASTM D7905/D7905M – 14.

[43] J. Schellekens and R. De Borst. Free edge delamination in carbon-epoxy laminates: a novel numerical/experimental approach. *Composite structures* 28, (1994) 357–373.

[44] L. Lagunegrand, T. Lorriot, R. Harry, H. Wargnier, and J. Quenisset. Initiation of free-edge delamination in composite laminates. *Composites Science and Technology* 66, (2006) 1315–1327.